# Automated Inspection of Sintered Uranium Fuel Pellets

by

Joe Vanderlaan

Bachelor of Engineering, University of Ontario Institute of Technology, 2008

A THESIS SUBMITTED IN PARTIAL FULFILLMENT OF THE REQUIREMENTS FOR THE DEGREE OF

Master of Applied Science

in

The Faculty of Engineering and Applied Science

Mechanical Engineering

| | |
|---|---|
| Supervisor(s): | Scott Nokleby, Faculty of Engineering and Applied Science |
| Examining Board: | Remon Pop-Iliev, Faculty of Engineering and Applied Science |
| External Examiner: | Ed Waller, Faculty of Energy Systems and Nuclear Science |

THE UNIVERSITY OF ONTARIO INSTITUTE OF TECHNOLOGY

November 2011

# Abstract

A method of applying high-speed, non-destructive testing technologies to the inspection process of $UO_2$ (uranium dioxide) fuel pellets is presented. The scanning process examines the surface of each pellet for correct manufacturing parameters. In this work, three inspection technologies have been investigated: laser scanning of surface roughness, 2D laser scanning of surface cross-section, and CCD camera inspection of surface integrity. The complete circumferential surface of each pellet is inspected using a combination of these three technologies. Both static and non-static test results on pseudo pellets are presented. The results show that the proposed technologies are capable of performing the necessary inspections.

# Dedication

To the ones I love,

*"I believe that to have a friend, a man must be one.*
*That all men are created equal and that everyone has within himself the power to make this a better world.*
*That God put the firewood there but that every man must gather and light it himself.*
*In being prepared physically, mentally, and morally to fight when necessary for that which is right.*
*That a man should make the most of what equipment he has.*
*That 'This government, of the people, by the people and for the people' shall live always.*
*That men should live by the rule of what is best for the greatest number.*
*That sooner or later ... somewhere ... somehow ... we must settle with the world and make payment for what we have taken.*
*That all things change but truth, and that truth alone, lives on forever.*
*In my Creator, my country, my fellow man."*

- Fran Striker -

# Acknowledgements

My thanks to my advisor Dr. Scott Nokleby. He provided technical guidance, major support, and grants towards the completion of this thesis.

I would like to thank Cameco for providing financial support for this research and prototype through the Cameco Research Chair in Nuclear Fuel at the University of Ontario Institute of Technology (UOIT). Cameco Fuel Manufacturing (CFM) are also thanked for their support of this work. In particular, I would like to thank Paul Knott, Dave Larkman, and Aniket Pant who served as contacts with CFM and provided information vital to this project. A final thanks to Marc Topalian and Keyence Canada for lending the 2D laser profile scanner for pre-liminary testing.

# Table of Contents

# List of Tables

# List of Figures

# Chapter 1

# Introduction

The nuclear energy sector is reliant on a continuous supply of nuclear fuel pellets for its sustained power production and growth. Thus it relies on an industry dedicated to the manufacturing of various fuel types. Regardless of the composition of the fuel, the standard developed over the years has been to form the fuel into cylindrical pellets, which can more easily be packed and stacked into reactor fuel bundles. The fuel composition being investigated in this thesis is of $UO_2$ in the form of sintered ceramic pellets, produced by Cameco Fuel Manufacturing (CFM); a division of Cameco Corporation. Currently, CFM employs a hybridized manufacturing process that involves both automated and labour based work cells. The process that CFM uses for producing the pellets has been standardized, however, with the advent of new technologies; the opportunity exists for the process to become more automated. Specifically, automation can allow the manufacturer to include more precise and efficient methods of quality control in the manufacturing process and will limit worker exposure to radiation.

The current method of quality control uses a point contact profilometer to measure the surface roughness of a pellet; this is performed at random points throughout different production runs. All other inspections of the surface of pellets are manually

performed via visual inspection and compared to a specific set of standards.

This thesis will investigate the identification and validation of technologies for measuring and quantifying the surface integrity of a fuel pellet. These results formed the basis for the design and development of an automated inspection system. The design of the automated system is presented in design report document [1]. The testing of the automated system prototype is discussed in this thesis.

The challenge of this project will be defined in two parts; with a general statement of the need for the project and then a statement describing the problem faced undertaking this project. The need for this project will be examined by focusing on the benefits that it will provide to the manufacturer. For the problem faced, the parameters posed by the manufacturer will be presented, to create an understanding of what is required by the scanner. Based on this, a set of requirements has been devised for the final design of the inspection system. The known system requirements will be described and separated into two categories; physical requirements and functional requirements. In the discussion, the physical and functional requirements are examined formally using opportunities, assumptions, and constraints. By doing so, it is possible to organize ideas, brainstorming work, and background research to allow for early dismissal of sub-par designs and the generation of the most appropriate design concepts.

## 1.1 Need Statement

The quality control process requires that the surface of each sintered $UO_2$ pellet must be examined for the specific reason of functionality of the product. The fact that must be highlighted is that the qualities of the surface of the pellet can be correlated to the surface integrity of the pellet. The integrity of the pellet is whether or not the pellet contains flaws, imperfections, or is smooth enough to be packed. If a pellet does not have proper integrity, it can lead to a failure of the fuel bundle. Inside the

reactor, the fuel bundles are subjected to extremely high pressure. This collapses the zirconium alloy tubes holding the pellets together and to the inner surface of the tube. With a lack of integrity, the pellet will not be able to withstand this high force and the zirconium alloy could fail from a rupture or a collapse and in doing so can cause contamination of the reactor. The smoothness of the surface will determine the efficiency of the tube, with it increasing as the micro contact points between alloy and the pellet surface increases. Thus the overall performance of the fuel bundle can be ensured by having high quality and precision made, sintered ceramic fuel pellets. These factors present a need for a quality control process, located after the surface grinding of the pellet has taken place in the manufacturing process. To be specific, the need is for an automated device to scan the complete circumferential surface of the pellet; in order to measure and quantify the surface integrity. Based on this, the objective will be to develop an automated system that monitors the qualities of the pellets in close to real-time; rejecting any pellet which does not meet the requirements. An additional note is that the nature of the pellets themselves are radioactive. The pellets produce low amounts of radiation, that is not directly harmful, but long term exposure should be limited [2]. Therefore it has been deemed advantageous to reduce the amount of direct material handling and the amount of direct worker presence required in the pellet manufacturing process. In addition, having an automated device can potentially be less expensive to run and maintain than employing a workforce over time. An automated system can reduce the amount of low quality pellets; possibly allowing the manufacturer to charge more for a better pellet or charge less for any savings that are realized. Lastly, on the user end, the automated system can provide verification of the quality of a specific stack of pellets. This could potentially absolve the manufacturer from the risks and consequences associated with reactor fuel bundle failures.

## 1.2 Problem Statement

This section will outline the problem associated with the design of an automated Non-Destructive Testing (NDT) system for the quantitative selection of ceramic $UO_2$ pellets using passing and failing of particular inspection criteria. The main objective for this project will be to determine different technologies that can be used to get a type of feedback that is useful for detecting the particular inspection criteria. In this case, the criteria can be generalized in such a way that a GOOD pellet has two main criteria to be met, where if they are not met; the pellet is categorized as BAD. The first criterion is characterized such that the surface of the pellet must be complete and have a smoothness of approximately 0.800 $\mu$m [3]. The second criterion is determined as: the pellet has no defects or flaws, which consist of the following:

1. Chips
2. Cracks and End Cracks
3. End Squares
4. Pits
5. Inclusions
6. Wheel Marks
7. Non-Cleanups

The specifics of this list can be seen in the Quality Verification Instruction (QVI): Fuel Stack Inspection [3]. Therefore the automated system must have some logically means of characterizing the received signals of feature extraction; in order to discern if the pellet meets the two GOOD criteria. This desired effect is similar to that of a filter; keeping out the large surface variances, while allowing smaller variances to pass. The system will aim to do this, while keeping up with a production scanning rate of

about five pellets per second in an inline conveyor type production line scenario. It will have to detect smoothness at up to 0.001 $\mu$m accuracy and the aforementioned surface defects at an accuracy of 0.01 mm$^2$. All the measurements must occur in-line in real-time or close to real-time rate, allowing each pellet to be scanned with recognition of the position in queue of the respective pellet. Based on the position of the pellet, the automated system will also have to indicate whether or not to reject each pellet scanned, which must happen without any further damage to the pellet.

## 1.3 Requirements

This section will identify the requirements of this project in relation to the design and implementation of an automated high speed scanning system. The goal of the system will be to ensure high quality and overall integrity of the surface of each pellet that is manufactured. In order to do this, the scanning system will perform in close proximity to the pellet surface, while not damaging or altering it in any way. This is to be done at an approximate rate of five pellets per second in a close to real-time scenario. The surface roughness should be measured to an accuracy of 0.001 $\mu$m and defects should be identified as small as 0.01 mm$^2$. A GOOD pellet is classified as having no flaws above 0.5 mm$^2$ and a surface roughness of approximately 0.7500 $\mu$m $\pm$ 0.0500 $\mu$m. Any pellet not fitting the aforementioned criteria is classified as BAD and is signaled to be rejected from the system; for possible reworking or recycling. The system must be able to track the position of the pellet within the system and will have the appropriate small sized footprint to be placed in-line after the grinding process. If all the above requirements are fulfilled by a single design, it should be chosen above others as it will ensure that the system fully performs to its expected goals.

### 1.3.1 Physical Requirements

The necessary states of being or how the system design is fulfilled, are also known as the physical requirements. They are as follows:

1. A pellet should remain motionless during scanning or the scan should account for a moving pellet.

2. Each scanned and rejected pellet must be handled so as to not cause any further damage to the pellet.

3. A method of detecting the spatial positioning of the pellet on the conveyor belt should be employed.

4. The system is required to operate in a manufacturing environment for ceramic $UO_2$ pellets.

5. The scanning system must have the appropriate small sized footprint to be placed after the grinding process.

In order to achieve a successful design the physical requirements should be followed closely if not satisfied completely. There are other variables that must be considered in the design, as they will affect the end design. These variables are discussed below in terms of the opportunities, assumptions, and constraints considered in the design.

**Opportunities**

The design process allows for the investigation of opportunities related to the physical parameters of the systems design. In the case of this system's design, the first opportunity presented is using a non-contact method of NDT for testing the integrity of the pellet to increase the rate of testing. As far as the specific NDT methods, a form of wave propagation that is complimentary to the uranium pellets can be implemented. By achieving a sufficient signal-to-noise ratio, the system can detect the presence of surface structures and thus the integrity of the pellet. In addition to

increasing the accuracy of how the pellet is rejected from the measurement system, a method of tracking the spatial positioning for each pellet must be implemented. This would ensure that the correct pellet is ejected when a BAD pellet triggers the scanning system. Tracking of the pellet will require the logging of data and thus an opportunity to record all data related to each pellet is presented.

**Assumptions**

Presenting the physical requirements brings to light assumptions that are made about the physical parameters of the system's design. These are made in order to create a design that is not redundant in any way. In this specific process there are very few defective pellets, making the normal pellet having a classification of GOOD. A pellet which has any combination of flaws or too high of roughness will be classified as a BAD pellet. Out of the total production, the estimated percentage of defects can be seen in Table 1.1.

Table 1.1: Percentage of Flawed Pellets

| Flaw Type | Percentage (%) |
|---|---|
| End Squares | 3 |
| Chips | 2 |
| Cracks | 0.5 |

**Constraints**

Since this is a manufacturing operation there are specific constraints involved when considering the physical design requirements, as well as some specialized ones. The physical constraints are as follows:

- The size of the automated device must be of dimensions to accommodate the current process setup.
- The interference from the surrounding workspace/environment.
- The small dimensions of surface defects and roughness.
- The reflectivity and permeability of the surface of the material.

These are important factors to consider in the design process because they in fact dictate what solutions can and cannot be implemented to solve the problem. If a solution or design does not fit the constraints, then the implementation of the developed system will most likely fail.

### 1.3.2 Functional Requirements

The necessary actions for the system design to fulfill are also known as the functional requirements. They are as follows:

1. The system should perform a scan of the surface of the pellet to determine the integrity and smoothness of the surface.

2. The method of scanning should not alter the surface structure while scanning for defects or surface roughness and should maintain a close proximity to the pellet itself.

3. The system will detect the integrity and roughness of the pellet in a close to real-time scenario at a rate of five pellets per second.

4. The roughness of the pellets should be measured with an accuracy of 0.0001 $\mu$m.

5. The system must proportionally discern and classify received data for every pellet into two categories; GOOD or BAD.

   GOOD pellets will be classified as having no surface flaws and a surface roughness of approximately 0.7500 $\mu$m $\pm$0.0500 $\mu$m [3].

   BAD pellets are classified as having the following defects or flaws:

   (a) Chips (see Figure 1.1)

   (b) Cracks and End Cracks (see Figure 1.2)

(c) End Squares (see Figure 1.3)

(d) Inclusions and Pits (see Figure 1.4)

(e) Wheel Marks (see Figure 1.5)

(f) Non-Cleanups (see Figure 1.6)

6. A BAD pellet should be rejected from the online manufacturing process for possible rescanning and reworking.

In order to achieve sufficient quality control, the given requirements and QVI [3] must be fulfilled in the design of the scanning system. However, there are some other variables that must be considered, as they will also affect the end design parameters. These variables will be discussed below in terms of the opportunities, assumptions, and constraints considered in the design.

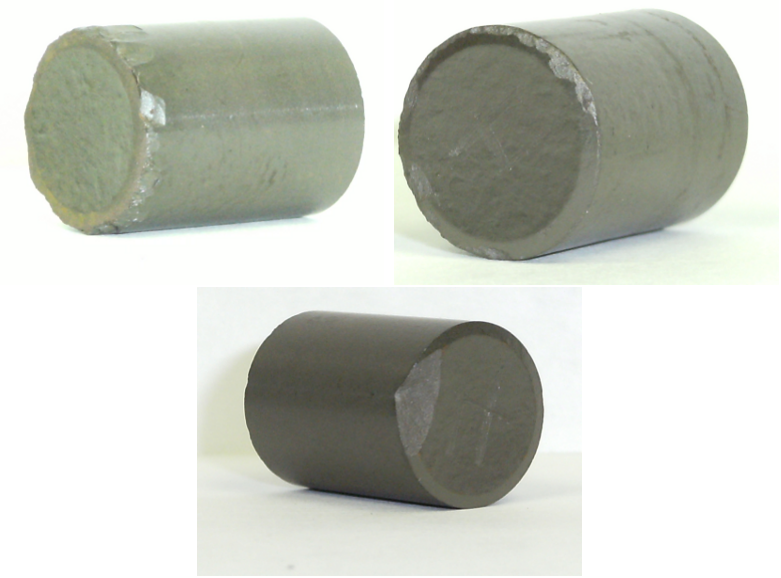

Figure 1.1: Pellets with "Chip" Defects

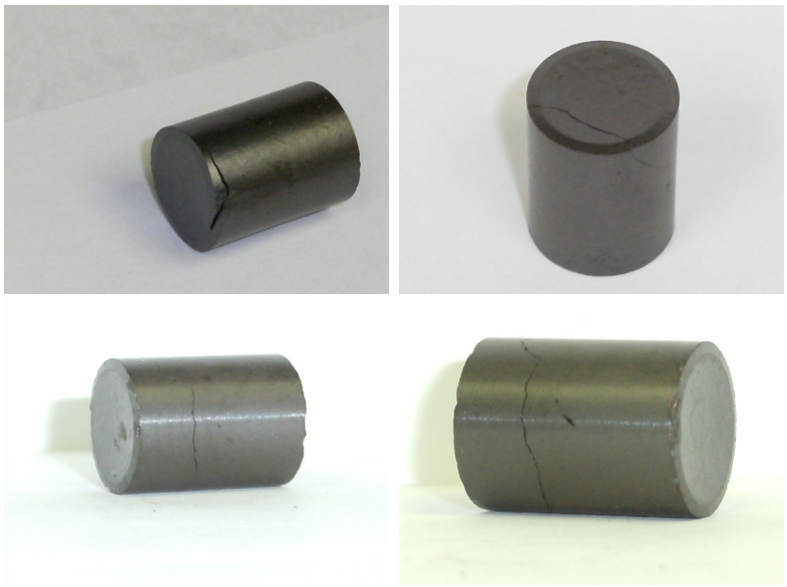

Figure 1.2: Pellets with “Crack” Defects

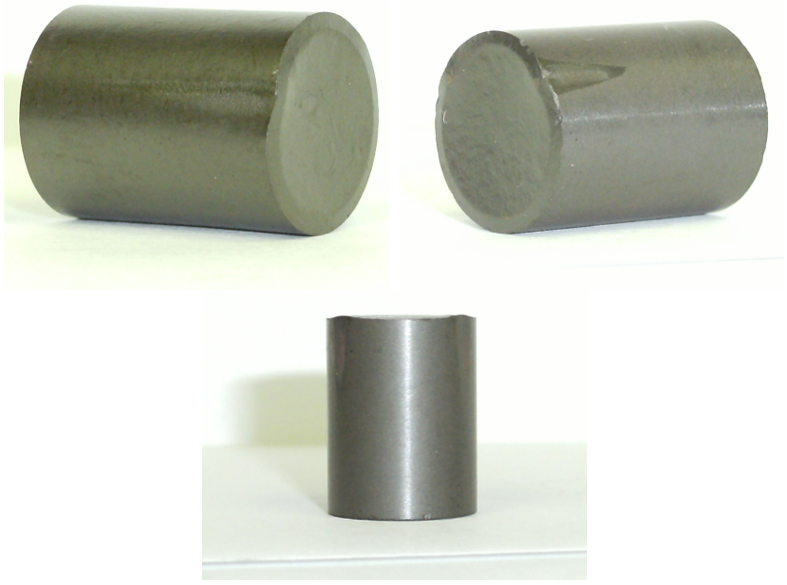

Figure 1.3: Pellets with “End Square” Defects

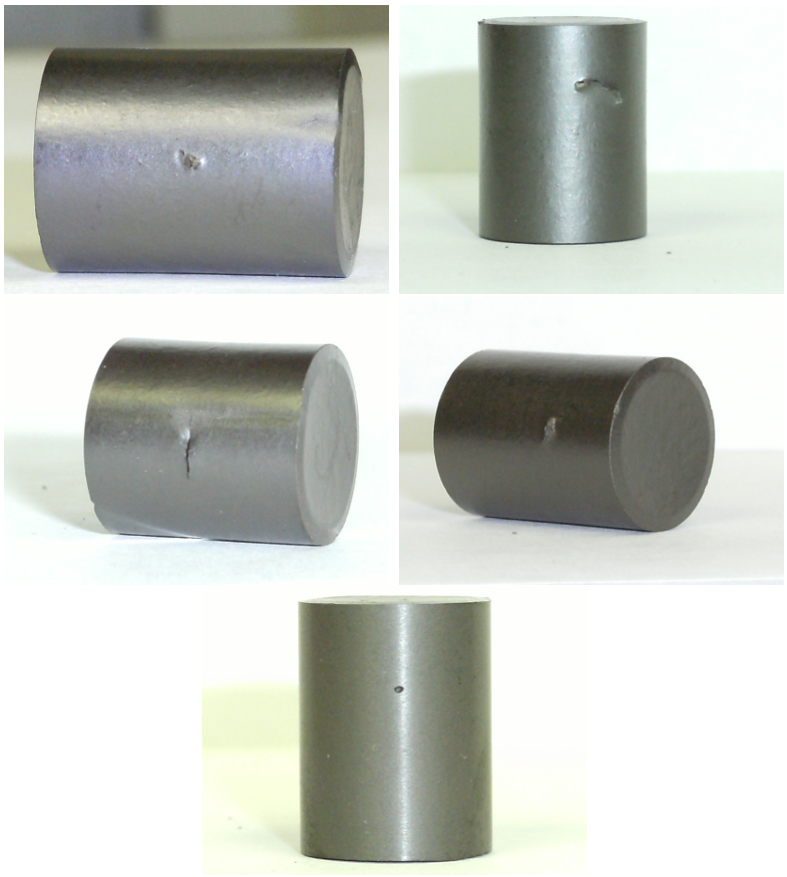

Figure 1.4: Pellets with “Inclusion and Pit” Defects

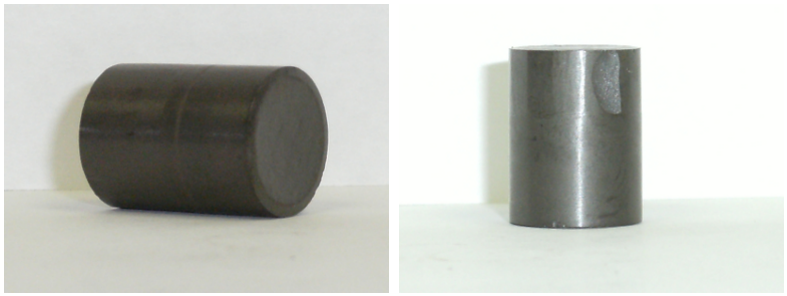

Figure 1.5: Pellets with “Wheel Mark” Defects

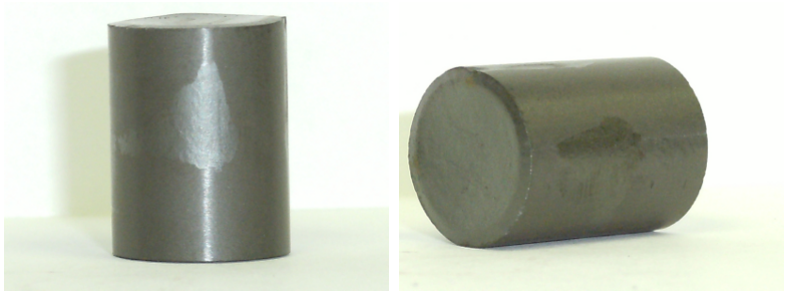

Figure 1.6: Pellets with “Non-Cleanup” Defects

**Opportunities**

In the design process, research on the presented problem is carried out in order to investigate if the problem has already been solved or what options there are to fullfill the design. This can also be considered as the opportunities that are available in order to solve the design problem. In the case of the automated scanning system there is a distinct opportunity to use proven NDT methods and update the technology that is incorporated with each method. The use of modern technology also presents a chance to find a solution that is most reliable and requires as little processing as possible, using the data in its rawest form. Another key point in terms of accuracy is the possibility of using MEMS based technology to develop a detection device, thus achieving a high degree of accuracy via the micro-sized technology.

**Assumptions**

In the most basic terms, this design is for the implementation of a quality control device for detecting the integrity and surface roughness of the pellets via an automated scanning system. This system will be placed in an in-line position in the pellet manufacturing environment. It can be assumed that this application will be high speed and a form of NDT will be applied in the inspection of the pellets. It will be assumed that only ceramic pellets of relatively uniform surface composition will be tested. It should also be assumed that if a pellet has appropriate surface roughness, then it should not have any defects or flaws. This should be noted to be true since any defect or flaw will have a higher surface roughness than is tolerable by the design parameters. The last point to assume is that it is not necessary to obtain a true real-time measurement of the pellets integrity. This is true as long as the position of the pellet can be tracked within the system, in order to appropriately remove the pellets classified as BAD.

**Constraints**

Since this is a manufacturing operation there are specific constraints involved when considering the functional design requirements, as well as some specialized ones. The

functional constraints are as follows:

- The speed and quantity at which the pellets will be manufactured on a daily basis.
- Achieving sufficient accuracy to detect surface flaws and roughness of moving pellets.
- The ceramic pellets are subject to having brittle mechanical properties.
- The work environment contains acoustic, vibratory, and dust interference that can affect electronic instruments.

These are the main considerations or limiting factors, otherwise known as functional constraints, involved with this design. These are the most important factors to consider in the design process because they in fact dictate what solutions can and cannot be implemented to solve the problem. If a solution or design does not fit the constraints, then the implementation of the developed system will most likely fail.

## 1.4 Organization of Thesis

Chapter 1 presented a brief introduction of the need for the project; a statement of the project requirements, both functional and physical requirements, were presented. The above statements provide an understanding of the aim of the project and a comparative basis for the goal, that the proposed design sets out to solve. Chapter 2 presents relevant background research in the form of literature, patents, and technology surveys. The identification of viable scanning techniques and apparatus along with preliminary validation results will be presented in Chapter 3. A test plan for identifying defective surfaces and the results of these tests, using the automated prototype, are presented in Chapter 4. Chapter 5 provides conclusions and recommendations for future work.

# Chapter 2

# Background, Patent, and Technology Review

Many automated scanning systems for industry have been developed in recent years and have done so along with advancements in the respective technologies implemented. In the nuclear industry, the manufacturing of sintered uranium fuel pellets requires that stringent quality assurance processes be implemented. At CFM these tasks are currently performed by skilled labour persons, who are not only subjective in their review of the pellets, but they are not able to identify all the defects on the surface of any given pellet. Herein lies the need for an automated system to perform the necessary scans that will detect the defects of a fuel pellet. The fuel pellets are cylindrical in nature and the scanning techniques have thus been developed to inspect surfaces with this geometric feature. Many other industries also scan cylindrical objects, thus this particular segment of automated surface scanning has been steadily developed. The following will present information directed towards the quality assurance of manufactured fuel pellets and assemblies.

The information that is presented will include the background and technological reviews done for the design of a high-speed automated fuel pellet scanning system. The

requirements presented in Chapter 1 detail the specifics of what classifies a pellet as GOOD or BAD; in terms of pellet quality. The focus of this section is to bring to light, the past work that has been done and to serve as a benchmark for the final design of the proposed scanning system. This also provides the opportunity to apply any techniques or advantageous design methodologies that have been previously developed and validated in a modern manufacturing environment, to the design of the system. The objective of this review is to identify methods of discerning surface roughness and also to quantify surface integrity. In addition any other applicable methods for detecting or classifying surface defects will be examined. This will be done via a literature, patent, and technology review.

## 2.1 Background Literature Review

The first section discusses the literature that was reviewed concerning the analysis of quality. They can be grouped into four major categories. The categories range from defect detection to pellet composition and homogeneity. The categories will be discussed as follows: irradiative techniques, acoustic techniques, optical techniques, and advanced classification techniques.

### 2.1.1 Irradiative Techniques

One of the techniques being used to examine uranium fuel pellets has been found to be the application of the radiographic absorption principle. This is accomplished by using gamma ray radiography; to evaluate the shape, size, density, and composition of a fuel pellet.

In Lehmann et al. [4] a method of determining the enrichment of isotope U-235, the homogeneity distribution of other neutron absorbing additives, and an averaged profile and diameter is presented. This was done using neutron sensitive imaging plates at

the NEUTRA station of SINQ (Swiss Spallation Neutron Source). The plates provide a way to measure the amount of neutron absorbance for each pellet. The relative intensities can be plotted versus the position of the pellet and can be qualitatively and quantitatively examined to verify the properties of the pellet stated above.

Similar techniques of gamma ray radiography have been presented by Muralidhar et al. [5], Badawy et al. [6] and Panakkal et al. [7].

Muralidhar et al. [5] and Badawy et al. [6] use passive gamma scanning techniques to examine completed fuel rods, with a Cobalt-57 collimated source and a NaI(Tl) detector. The rods are examined for stringent specifications, such as pin length, placement and loading of internal mechanism, and the density of the fuel and insulation pellets.

Panakkal et al. [7] similarly proposes an x-ray film technique where radiation emitted by the fuel is captured and stored on an x-ray film cassette. Gamma autoradiography is then used to examine the cassette, producing an image where the optical density is proportional to the degree of enrichment of $PuO_2$. This reveals both quantitative and qualitative results; for composition, detection of incorrect loading, and the presence of plutonium rich agglomerates in the outer regions of the fuel pellets.

### 2.1.2 Acoustic Techniques

Swart et al. [8] propose a method for determining macroscopic surface roughness based on the scattering geometry of acoustic waves reflecting off an imperfect surface. In this work, the surface variance of the asphalt of a road surface of any type is examined. An acoustic transducer is used to generate sound waves that reflect of the road surface. Normalized Fourier spectrum analysis is then used to measure the reflection of the scattered waves in the specular direction on an acoustic broadband reciever. Aggregates of different sizes were screened and formed into 1 $m^2$ sections that were then validated with the ultrasonic measurements (see Figure 2.1).

In Courtney et al. [9], the use of bispectral analysis techniques of ultrasonic waves

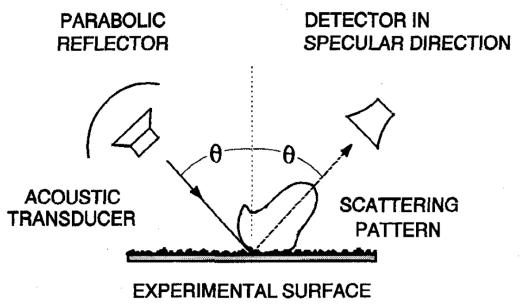


Figure 2.1: Representation of acoustic techniques for determining macroscopic surface roughness [8]

through engineering components, for crack defect detection, is discussed. A pair of sinusoidal ultrasonic signals are summed and amplified into the test piece, exciting a piezo-ceramic disk bonded to the test piece with a cynoacrylate adhesive. The signals were measured and digitized using Fourier transforms, allowing for bi-spectral signal analysis for any non-linearity; which result in cracks being detected.

Panakkal et al. [10], describe a method for monitoring ultrasonic velocities in a pellet; in order to extrapolate the density of the pellet. The measurement was done by a Krautkramer CL 204 ultrasonic velocity meter, averaged over 10 measurements, coupled by Exosen 7 couplant. It is said that any voids or porosity in a pellet will have such an effect as to slow down the ultrasonic waves and must be accounted for, since the derivative of the elastic modulus (M) is greater than unity for the pellet.

### 2.1.3 Optical Techniques

The most prevalent technique that has been developed for quality assurance purposes has been digital imaging or machine vision systems. These systems are comprised of an image sensor and a light source, where the effective image is captured, digitized, and then analyzed for specified characteristics. Information has been found on the geometric and physical relationships of light to surface reflections and how they can be expressed mathematically. Techniques utilizing laser light to measure surface

roughness of ceramic materials has also been found as it is applicable to the surfaces of sintered fuel pellets. Finally techniques for traditional light scanning surface inspection of cylindrical products and fuel pellets will be discussed.

Nayar et al. [11] go into detail about the development of accurate reflectance models and how they can greatly benefit machine visions systems. In this work the Beckmann-Spizzichino (physical model) and the Torrance-Sparrow (geometric model) are described in detail and the validity of each model is stated. By examining the reflectance curves predicted by the two models, a 'reflectance framework', comprised of three components, has been developed. The effects of surface roughness on the three components are analysed in detail; the components are: the diffuse lobe, the specular lobe, and the specular spike. It is noted that in order for these models to be valid, the wavelength of the incident light must be considered small in comparison to the dimensions of the surface imperfections.

There have been two papers found to discuss the measurement of surface roughness of ceramics using a non-contact laser reflectivity (LSR) measurement technique. Whitehead et al. [12] describes and compares two methods of assessing surface finish of ceramic surfaces: contact stylus tracing method and the LSR method. The paper states that in ceramics, unlike metals, there is little correlation between RMS (Root Mean Square) and Ra (Average Roughness) optical roughness. It also states that a surface cannot be characterized with the measurement of Ra alone, other techniques should be used to asses other characteristics; such as the profile of the surface.

Similarly, Jolic et al. [13] discuss current surface roughness measurement techniques for ceramics and present a comparison with an optically based technique. The paper outlines the general design strategy for the LSR technique, using a 0.1 mW 632.8 nm helium-neon gas laser, to create a scattering distribution. The images were then processed using roughness measurement algorithms to calculate surface roughness, in what was shown to be a reliable manner (see Figure 2.2).

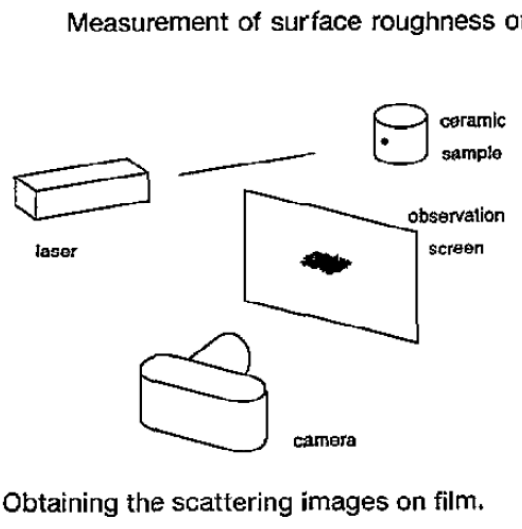


Figure 2.2: Representation of surface comparison discussed it Jolic et al [13]

A novel approach to scanning continuously extruded cylindrical products has been presented in Stefani et al. [14]. An initial overview of current surface inspection technologies is presented and compared to a novel design. The novel design uses a conic reflector to collect collimated light on the opposing side of the cylindrical body, from the light source. The collected light is focused onto a single photo-diode, which is used to measure the output voltage of the collected light. A surface defect is said to cause the light to scatter and thus will cause a deviation in the output signal, which can be compared to threshold values of acceptable surface deviation limits.

Finogenov et al. [15] present the results of the development and testing of an automated inspection system based on the aforementioned method of surface inspection. High contrast images of pellet surfaces are created for defect and comparative analysis, taking into account defect area and length. The system was shown to work with high efficiency and was able to detect the defective pellet from lots of 100 pellets.

Lichauer et al. [16] propose using a fluorescent light source to illuminate the surface of the pellet, while using a line scan camera and an image acquisition system to digitize an image of the pellet surface. In addition, the paper outlines the problems

associated with monitoring the surfaces of pellets at a processing rate of 10 MHz or greater. Thus methods of image skew compensation are also discussed, along with the proposed methods of defect detection. The paper reports defect detection rates of 97% at a pellet scanning rate of up to 7 pellets per second.

### 2.1.4 Advanced Classification Techniques

The methods of surface inspection that have been discussed, detail the technologies or the techniques that could be used. The classification of defects in these works have been slightly rudimentary, with a few papers discussing some defect detection algorithms. Thus, information on more methods of classification for defect detection technologies was investigated. In particular Bayes classifiers, subtractive clustering and Sugeno fuzzy inference, and neural network applications have been reviewed [17] - [19]. Fischer et al. [17] and Hayajneh et al. [18], present methods for failure detection systems in power generator overheating and expected drilled hole quality based on feedback measurements, respectively. Both works demonstrate the improvements of advanced classification techniques in error detection over more common place ones. The third work, Keyvan et al. [19], aims to present finding on the inspection of fuel pellets using an artificial neural network. The paper examines three kinds of neural network architectures and evaluates their performance to detect good versus bad pellets. It was found that an artificial neural network can receive adequate training data and achieve a high success rate of classification using machine vision.

## 2.2 Patent Review

Following the review of the literature relevant to the quality assurance of the surface of sintered ceramic fuel pellets, a review of viable and applicable patents was conducted. All patents presented concern some quality inspection technique of nuclear fuel pellets.

The patents are oriented to scan pellets for correct density, shape, and for the presence of defects.

### 2.2.1 Density Measurement and Analysis

Hill et al. [20] present a method for determining the density of a nuclear fuel pellet using gas displacement. This method involves three main steps, beginning with the measurement of weight of the pellet and the pressure of a reference volume of gas that has isothermally expanded into a manifold. Next, the pellet is placed within the manifold and the pressure is again measured, using the same reference volume. The pressure difference is then shown to yield the specific density for the object placed inside the manifold, in this case the fuel pellet.

### 2.2.2 Pneumatic Defect Detection

A method for detecting surface defects using a pressurized gas was presented by Miller, Jr. et al. [21]. The gas jets are directed into a central bore where the pressure generated on the surface of a pellet is measured by multiple transducers within a ring. Any deviations in pressure between pneumatic circuits pass a threshold amount will signify that a defect is present.

### 2.2.3 Dimension and End-Square Verification

Another technique presented by Wilks et al. [22], uses LVDT's (Linear Variable Differential Transformer) to measure multiple points of displacement on various points of swivel plates contacting the end of each fuel pellet. The multiple points of displacement can be used to construct a geometric plane to represent the swivel plates. The perpenidicularity of the two end plates for a pellet can be verified, thus indicating the degree of end-squareness, as well as average length for any given pellet.

### 2.2.4 Ultrasonic Defect Detection

Ahmed et al. [23] present a method for evaluating the presence of surface defects for a fuel pellet using reflected acoustical energy. This implements an ultra-sonic technique for evaluating the presence of surface defects using an array of sensors or transducers to measure the reflection of energy off of the surface of the pellet (see Figure 2.3). A pellet inspection chamber is designed so that a consistent propagation of sound waves can be achieved for each pellet. Thus the system can be used to measure the reflections of acoustical energy and compare the measured values to previously measured standardized pellets. This type of comparison is able to distinguish a difference between the surfaces of pellets, but is not able to associate specific measurements to their respective defects; it is limited in this way.

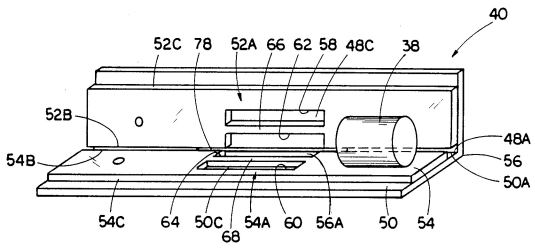


Figure 2.3: Representation of Ahmed et al Ultrasonic Device [23]

### 2.2.5 Optical Defect Detection

The most prevalent method found for scanning fuel pellets was the use of digital imaging devices to visually inspect a pellet by measuring intensities of reflected light. Patents [24] to [33] use variations of basic reflectometry techniques to detect defects with an image sensor, an example of which can be found in Figure 2.4. This technique works by illuminating the surface of the pellet with a light from a standard source; using mainly, a ring light source or a collimated light source. The light hits the surface of the pellet and is reflected in the specular direction correlating to the surface of the

pellet. For a non-defective pellet surface the majority of the irradiated light is reflected along the specular angle, whereas the reflection is diffused from the specular angle in the presence of a defect. Therefore the presence of defects can be detected by measuring the intensity of reflected light off of the surface of the pellet. The optical methods of pellet inspection are found to be oriented and limited to only evaluating the surface of a fuel pellet.

## 2.3 Technology Review

The following is a brief over look on the technologies that were investigated to suit the specification set out by CFM, to create an automated pellet surface inspection system.

### 2.3.1 Inductive Probe for Flaw Detection Device

A device has been found to look inside the profile of an object; the encircling probe and coil offered by NDT Technologies Incorporated [34]. This probe is a non-contact device that is used to measure the eddy currents that are generated within an object. The principle works upon the fact that a uniform solid will have a uniform distribution of eddy currents generated. This means that any deviation in the solid, via a defect, pit or scratch, will results in an undulation in the receiver signal. The undulation is of course an imperfection in the material, which can be related to a flawed material. This method is less than satisfactory for measuring roughness, since the principle it relies upon can only detect discontinuities. This means that if a surface is complete with any reasonably small roughness, it most likely will not have any detectable deviations in its signal. In order to use it to measure roughness, it would have to be compared to a set of 'good' waves or criteria that determine a 'good' wave. Thus this method is best used as a method to profile the surface to a degree as to discern whether or

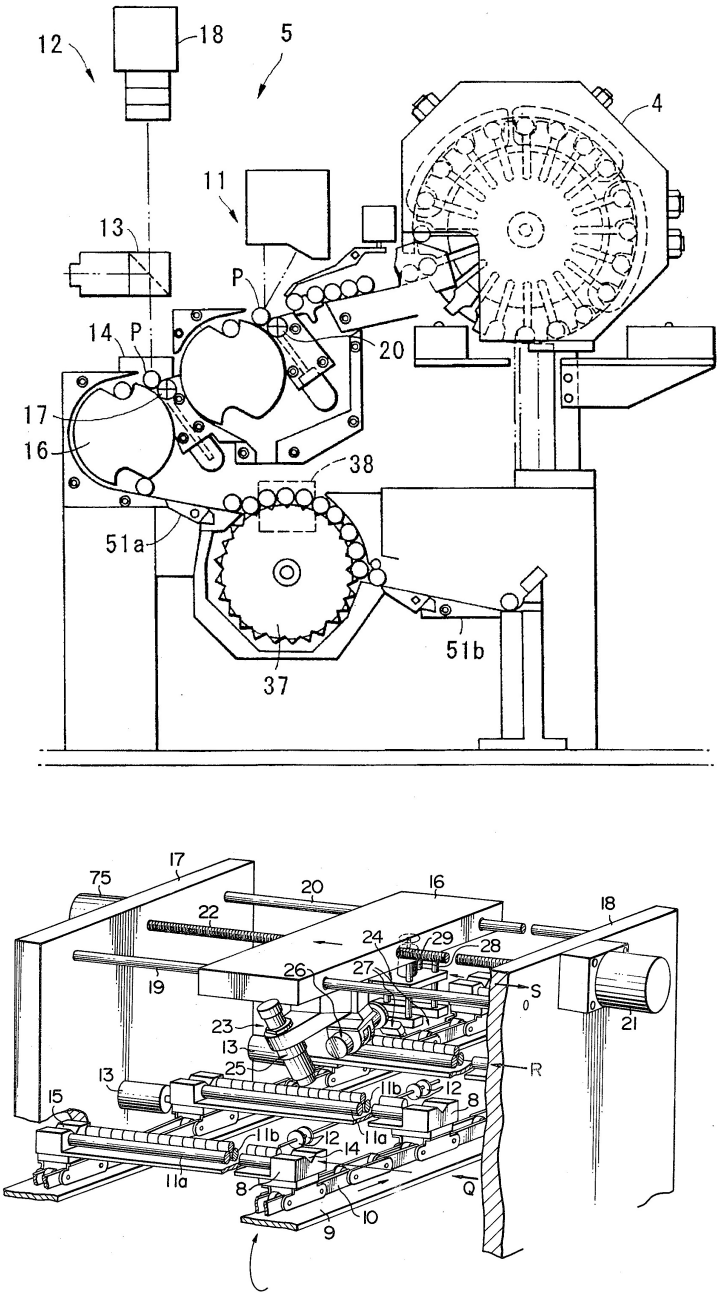


Figure 2.4: Representaion of various camera systems for scanning fuel pellets [29], [26]

not the surface is complete or incomplete. This is especially applicable to scanning of uranium pellets because they are slightly paramagnetic and thus are able to generate eddy currents when subject to a magnetic field.

### 2.3.2 Ultrasonic Probe for Flaw Detection System

Another type of probe has been found at GE Sensing and Inspection Technologies [35] for the measurement of ultrasonic frequencies through various materials. GE provides an ultrasonic flaw detector with a digital viewing unit, which can be used to view a time based receiver input. It is similar to the encircling probe in the types of imperfections it can find; however, it differs in the technology it uses to achieve the same outcome. As stated before the measurement of velocity of ultrasonic energy through a specific media can be used to identify defects. A defect is signified by non-uniformity in the measured reflected velocity of the induced ultrasonic waves. If the waves slow more than expected or the intensity is dimished, a defect is considered to be present.

### 2.3.3 Laser Surface Roughness Measurement Device

The first type of optical digital scanning that was found was a device to acquire the measurement of surface roughness, accomplished using point-laser profilometry. Optical Dimensions LLC builds surface roughness scanning equipment and the LaserCheck Model 6212C measurement device [36], has been found to achieve the desired results with the required accuracy. This device performs measurement of surface roughness by aiming a point-laser light at an object so that it has an appropriate angle of reflection off of the scanned surface to be read by a CCD image sensor.

### 2.3.4 2D Laser Profilometry Device

The second type of optical digital scanning is the measurement of the 2D profile of the surface of the pellet. This scan functions using laser light and measures the intensity of reflection of a line patterned laser light, which is comprised of many single points of laser light. An example of such a system is the Keyence LJ-G030 measurement head and controller [37]. This system can be used in the comparison of surface profiles.

### 2.3.5 Digital Imaging Device

The final optical scanning stage reviewed uses a CCD camera to capture a surface image; for digital processing. An LED light source is used to illuminate the surface. The intensity of the reflection is measured from the image sensor with a digital capture card in a PC creating a monochrome digital picture having varying degrees of dark and light coloured pixels. Software can be used to compare the captured image with reference images to identify defects on the surface of a pellet.

## 2.4 Summary

The purpose of the background, patent, and technology review was to recognize the relevant works that exist and to improve upon them. In this case the basic concept of scanning fuel pellets was targeted in this review, the results were presented in three sections targeting any literature, patents, or technological components that are accessible. The literature for scanning cylindrical objects covered irradiative, acoustic, and optical techniques, as well as advanced classification techniques. Following that, any accessible patent databases were searched for information pertaining or relating to the scanning of cylindrical pellets for surface defects. These patents included the measurement of pellet density and the use of pneumatics, lasers, ultrasonic, and optical systems for the detection of surface defects. Lastly, the available technologies

pertinent to this application were discussed and specific instruments were identified. These instruments included inductive and ultrasonic probes, as well as laser scanners and camera scanners. Based on these works the final design for an automated system has been developed and can be seen in the design report [1], the chosen instruments that have been validated can be seen in Chapter 3. The different scanning techniques and devices were chosen to best ensure the possibility of success, based on access to appropriate equipment for testing and on ones available knowledge base. In addition the scanners were chosen to satisfy the production speed; by having appropriate scanning rates, and they were chosen to have high resolution; to ensure that measurements achieved accuracy requirements for defects.

# Chapter 3

# Identification of Viable Technologies

In this chapter, the different methods of feature extraction will be proposed along with the technologies that can be used to evaluate them. The information will be presented in three categories. They are the scan of the surface shape of each pellet, the scan of the integrity of the pellet surface, and the scan of the surface roughness of each pellet. Each method of feature extraction will be described in terms of the identified technology, the device to be used, and the reasoning behind its validation and the corresponding validation test results. It should be noted that this is not necessarily the order in which the scans should occur or will occur in the automated system. This is due to the fact that the components along with the system layout will dictate the position and order of the methods. The important thing is that, at a minimum, all the scanning methods will occur in the assessment of each pellet.

Based on the research conducted and the literature review, three scanning techniques and devices have been identified for application in this project. To reiterate, the shape of the entire surface, the integrity of the surface, and the roughness of the surface will be examined for each pellet. This will be accomplished using the three

respective scanners that were identified. The following is an account of the reasoning and validation testing of the techniques and scanners. It is the supporting data to re-affirm the validation of each scanning technique and device. A test plan was developed and performed, it is presented below in the validation of each scanning device. The completion of each test according to the test plan was accomplished and the results were recorded. The results are presented and then discussed in order provide a verification of the validation; for each scanning technique and respective scanners. According to the data, it suggests that each of the techniques and devices will lend themselves to the design and development of the fully automated system.

The validation testing, as it was mentioned, is meant to provide the concrete proof for the validation of the scanning technologies. The validation tests have a secondary function, which is to prepare the scanning instruments for performing automated scans. This is accomplished with an initial calibration for each scanner, depending on which scanner is being evaluated. The calibration will allow the received signals from the scanner to be useful for the task at hand. It is carried out using a standardized set of calibration pellets that has been checked for acceptable pellet parameters and tolerances. An exception will be made with the surface roughness scan, as a set of verified calibration surfaces will be used to calibrate each scanner. Following the calibration of each scanner, each scanner is then tested for accuracy. These initial tests will reveal a lot about the scanners and how useful they are in this application. The tests show that each scanner is in fact validated for this application, whether or not it can measure defects, and lastly if anything is functionally wrong with any of the scanning devices.

## 3.1 Surface Shape

The first of the three feature extraction methods to be discussed is the method of recognition of surface shape for a test piece and the possible technologies that can be implemented. The end shape of the pellets is most important to the final stacking process because the pellets are laid end to end and must be in contact with each pellet in the stack. Maintaining a square end ensures that when a stack is measured its length is measured accurately and it also ensures that there are no gaps in the stack that could cause the tube to rupture. Also having a square end will fulfill the requirements document and thus the scan for this feature becomes necessary to ensure a quality pellet. Looking back to the literature survey, the technologies that can be applied are similar for the other methods of feature extraction, but they are being applied in a different manner.

The applicable technologies for extracting surface shape are differential refractometry and the use of digital imaging techniques. The first technology mentioned, similar to that which will be used in the last feature extraction method, was the use of differential refractometry. This implementation could possibly employ either the propagation of sound or light waves. Instead of using the specular angle of reflection to image ridges on the surface of an object, it will have to be used to detect the signal for a flat and square surface. This will require that the technology be set up in a linear array to become in effect a line scanner. By generating a line of propagated waves, there should be an opportunity to detect the presence of an edge, therefore allowing the extraction of the cross-section of the end feature of each test piece. Through signal processing and classification, the aerial view of the test piece should be enough to effectively determine the surface shape. A note should be made that if there is an end flaw or overhanging edge centered towards the top of the scan, it may obstruct the ability of the scan to discern a square end feature. This will only be the case if the flaw or overhanging edge does not slope to one side or if it is not rounded on the

end. If this is the case and a flawed pellet is classified as a GOOD pellet, the second identified feature extraction method will prove to be a legitimate backup for detecting any missed defects.

The other possible technology for detecting the surface shape is to use digital image processing to perform shape recognition. Using a digital imaging device, such as a CCD camera, the optical image of the test piece can be digitized. This technique can extract images at a very high rate using data features called pixels that can be either displayed or processed. This type of imaging is achieved in a non-contact scenario and can be done at high speed, due to its high capture rate.

There are various opportunities for adapting proven algorithms for detecting object shapes; to detect the end square shape, as well as other features. Of the available technologies, 2D laser scanning is the best choice. This scan functions using laser light and measures the intensity of reflection of a line patterned laser light, which is comprised of many single points of laser light (see Figure 3.1). It carries out scans with a non-contact method of feature extraction and can accurately provide a relevant measure of the cross-section of each test piece.

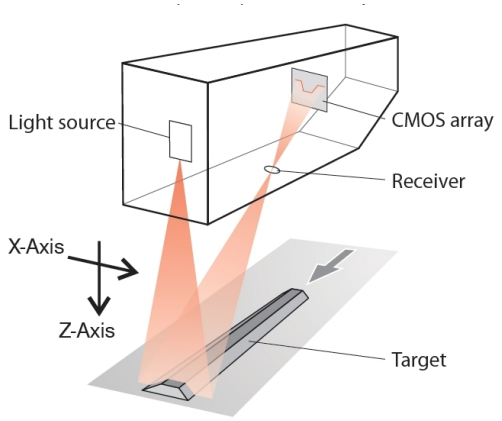


Figure 3.1: Representation of Laser Line Used in 2D Scanning [37]

### 3.1.1 Chosen Scanning Device: 2D Laser Scanner

A Keyence LJ-G030 measurement head and controller (see Figure 3.2) was identified for use in the comparison of surface profiles, based on superior performance characteristics over other similar devices. This device uses a CMOS sensor so that it is able to measure the intensities of individual pixels in the sensor's array. By measuring the intensities of groups of pixels, the controller is able to construct a 2D profile of the surface of an object. The details of the profile construction are proprietary, but the process is similar to measuring the distance for many points of reflection with the sensor, while accounting for any stray reflections as best as possible. The controller is able to use the measurements to build a very accurate profile of the surface being measured. It is also able to compare the measured surface profile to a reference profile with a precision of 0.001 mm. The controller is able to take the distance measurement of the many points along the profile and save the data for analysis purposes. A serial communications link is established in order to activate and deactivate the controller, as well as to receive measurement data. The comparative measures are performed on board the controller and a trigger can be initialized to activate any time that there is a non-comparable surface found. In addition, the information can be visually presented on an LCD monitor connected to the controller.

### 3.1.2 Validation

The test plan for validating the surface shape scan is comprised of an initial calibration of the 2D scanning head, followed by a test for operational accuracy of the device. The validation of the scan for the surface shape starts with an initial calibration of the 2D scanning head. This test will involve using each scanning head to measure the cross-sectional area of a standard surface of a known diameter and cross-sectional area. For calibration, the test will record the upper and lower limits of the measured cross-sectional area. By recording the overall upper and lower limit for each scanner,


Figure 3.2: The Keyence LJ-G030 TwoD Laser Scanner [37]

the averages of each scan can be used to derive an appropriate range of where to set the rejection thresholds of each scanner. By using the set of thresholds and setting up each scanner, the accuracy can then be evaluated.

The validation of accuracy for the 2D laser profiling was to recognize if a pellet surface is free of defects. This is done with the comparison of the standardized profile, shown in Figure 3.3, against the calibrated ones. It must be noted that all testing done in this thesis was on pseudo steel pellets painted in a matte-black. This test provides a 'pass' or 'fail' measurement, based on the degree of the coincidence between the test profile and the standard one. A measurement of multiple points of the profile can be taken, but is not necessary for this application. This is due to the fact that any deviation, either above or below a variance of a predetermined threshold, results in a defective pellet. The degree to which the size of the defects can be detected relies on the accuracy of the digital image sensor. For this test, a difference in the profiles down to 0.001 $mm^2$ can be seen. With the results, the average cross-sectional area and the standard deviation of each scanner will be calculated. The results should be analyzed to look for any measurements that are out of proportion to the expected results.

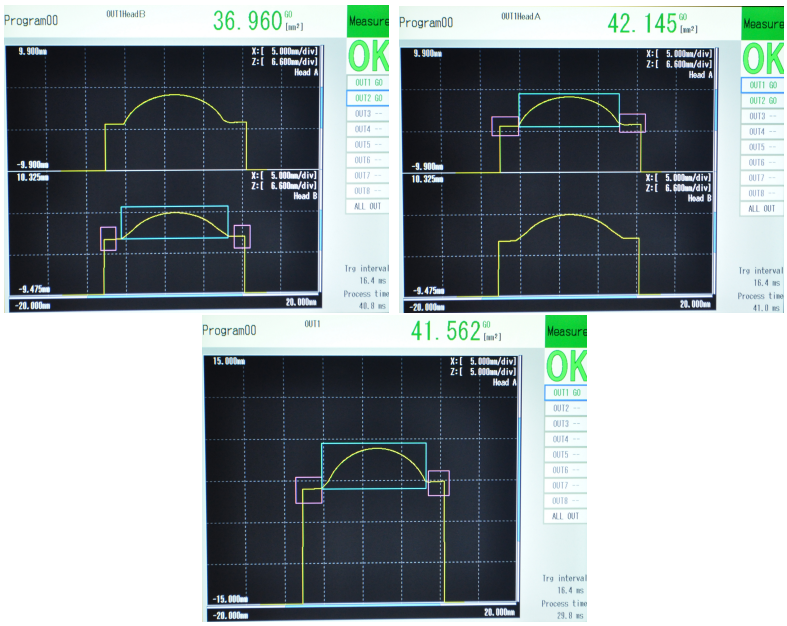


Figure 3.3: Standardized Profile of 2D Shape for Scanners 1, 2, and 3

### 3.1.3 Validation Results: Surface Shape Scanning

The initial calibration of the 2D laser scanning device consists of setting the master profile for each scanner and then the respective thresholds. The master profile must first be acquired using the calibration pellet. The acquisition basically stores the measurement of many points to the memory of the controller unit. It requires a simple setting chosen in the controller menu while the calibration surface is in the proper position and orientation. The results of setting the master profiles is shown in Figure 3.4. This is a necessary step to accomplish the type of comparison measurement that is required in this work. The reasoning for this is that it is the simplest method for discerning if a surface cross-section differs from the required surface cross-section within a specified parameter. Another method, such as mathematically examining each point of measurement or calculating the radius of many points on a surface, would be less efficient for examining the surface as a whole. If only one or a few features such as height differential measurements were necessary, then the other methods of measurement could be more suitable.

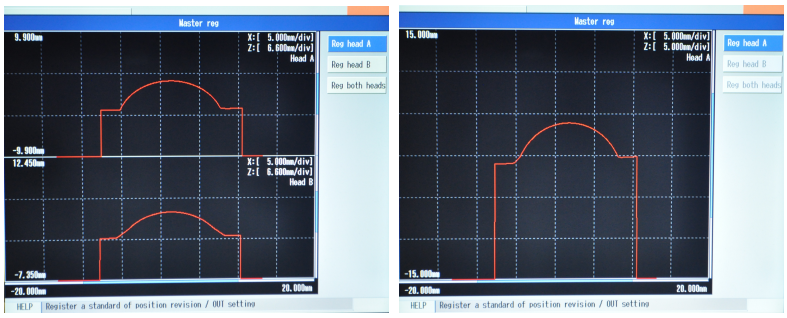


Figure 3.4: Master Profiles of 2D Shape for Scanners 1, 2, and 3

After each of the scanners is calibrated correctly to scan pellet surfaces, it is necessary to check for the accuracy of the system at detecting defects. In this case, the accuracy will reflect the amount of area of the cross-section that is being measured. To do this, it is first necessary to calculate the predicted measured values for each scanner. It should be noted that the scanner will be used to measure the area of a segment of the cross-section, dependant on the 'viewing window'; thus the predicted segment for each scanner is found. A diagram depicting the cross-section of a pellet can be seen in Figure 3.5, each of the segments are indicate by $A_1$, $A_2$, and $A_3$ for scanners 1, 2, and 3, respectively. The equation to calculate the predicted area of the segments is

$$A_{Segment} = A_{Sector} - A_{\theta_N/2} \tag{3.1}$$

where $A_{Segment}$ is the area of the cross-section that is being approximated, $A_{Sector}$ is the complete area of the from the center of the cross-section for the angle of sweep for a given 'viewing window', and $A_{\theta_N/2}$ is the remainder of the area that can not be approximated.

To provide a reference, a calculation of the total cross-sectional area of an ideal pellet and the area of each sector is done. The cross-sectional area is simply calculated as the area of a circle:

$$A = \pi r^2 \tag{3.2}$$

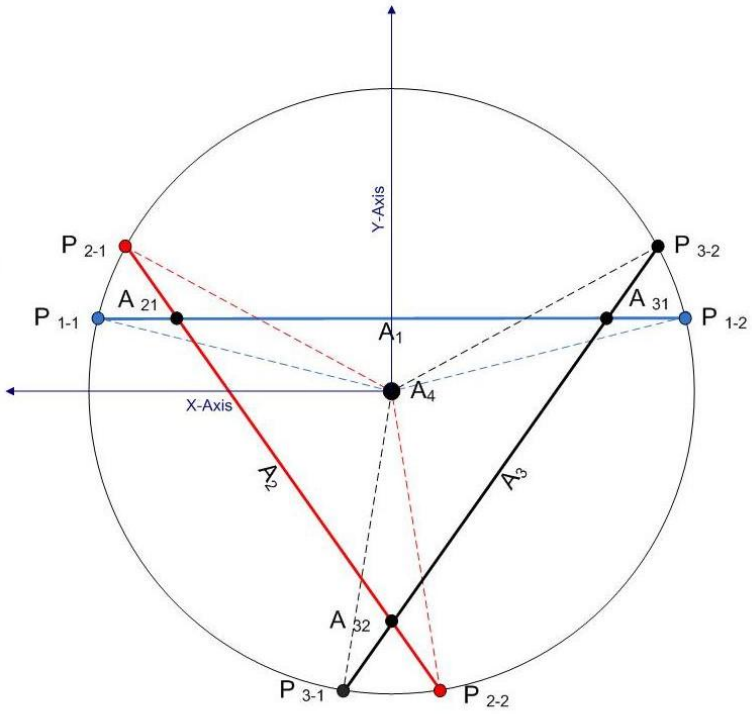


Figure 3.5: Diagram of Cross-Section of a Pellet Depicting the Measured Segments, Scan Overlap, and Void Scan Regions.

It was found that the approximate area of the cross-section of an ideal pellet is 132.732 $mm^2$ and that the sector of each 'viewing window' should account for more than at least one third of the total cross-sectional area; approximately 44.244 $mm^2$. Using these numbers as a reference, the calculated results for the sector can be seen below; using the following equation to calculate the area of the appropriate sectors:

$$A_{Sector} = \frac{\theta_N}{360}\pi r^2 \tag{3.3}$$

The calculated values for each of the sectors are as follows, all of which are expected to account for more than one third of the total area:

- Sector $A_1$: 53.562 $mm^2$
- Sector $A_2$: 47.931 $mm^2$
- Sector $A_3$: 47.931 $mm^2$
- Sector Total: 149.424 $mm^2$

Examining the results it can be seen that sector $A_1$ is 21.1% greater than one third of the total and sector $A_2$ and $A_3$ are each approximately 8.3% greater than one third the total area. This will result in a total overlapping in scans of approximately 12.6% greater than required. Next a perpendicular bisector will be used to divide the sector and create a triangle to calculate the resulting area of each respective sector minus the corresponding segment; the area is indicated as $A_{\theta_N/2}$. The total area of this triangle can be calculated by:

$$\begin{aligned} A_{\theta_N/2} &= \frac{1}{2}bh \\ b &= 2sin\left(\theta_N/2\right)r \\ h &= cos\left(\theta_N/2\right)r \end{aligned} \tag{3.4}$$

Now Equation (3.1) can be calculated for each of the identified segments. The calculated values for each of the segments and the total area of all the segments are as follows:

- Segment $A_1$: 39.984 mm $^2$
- Segment $A_2$: 31.748 mm $^2$
- Segment $A_3$: 31.748 mm $^2$
- Segment Total: 103.480 mm $^2$

Each of these segments now correlate to the appropriate sectors that account for the approximate overlapping scan. The total of the values can be compared to the total cross-sectional area minus the area of $A_4$; which is not measured by any of the scanners. To do this a Cartesian coordinate system was established and the points that each segment intersect with the outer circumference are found using the parametric equations of a circle,

$$\begin{aligned} x_P &= r sin\theta_P \\ y_P &= r cos\theta_P \end{aligned} \tag{3.5}$$

where $\theta_P$ is the cartesian angle of the point on the circumference of the circle. Then the corresponding points of each segment can be used to find the equation of the line for each segment based on the same Cartesian coordinate system. The equation of a line is of the form,

$$y_P = m_P x_P + b_P \tag{3.6}$$

where $m_P$ is the slope and $b_P$ is the intercept, of the line, for two corresponding points as shown in Figure 3.5. Using substitution and both points of intersection of each segment with the circumference, the equations of the line for each segment can be calculated. They are found to be:

- Segment $A_1$: y = 2.223
- Segment $A_2$: y = 1.428x - 4.789
- Segment $A_3$: y = -1.428x - 4.788

Using corresponding equations for lines, they are set to equal each other to solve for the 'y' coordinate and substitution to calculate the 'x' coordinate for the points of intersection of each line. The three points of intersection will make up the vertices of $A_4$. The results of calculating the points of intersection are shown in Table 3.1, these points can finally be used to calculate the area of the center region. This is accomplished by using the equation for calculating the area of an irregular polygon,

$$A_{Triangle} = \left| \frac{(x_1y_2 - y_1x_2) + (x_2y_3 - y_2x_3) + (x_3y_1 - y_3x_1)}{2} \right| \tag{3.7}$$

which in this case is an irregular triangle. The calculation reveals that the area of region $A_4$ is approximately 57.089 $mm^2$. By subtracting this value from the total cross-sectional area, the total area covered by the segments can be validated as being bigger than the segments created by dividing the cross-section into thirds. The value of the segments would then be calculated to be 75.643 $mm^2$, which is smaller than the total area of the predicted segments; that correlate to the 'viewing windows', which is 103.480 $mm^2$. This accounts for an overlapping of approximately 36.8% for the segments. Compared to the overlapping of the sectors, which was found to be 11%, there is a difference of approximately 26%. Thus the null area skews the percentage difference in area of the overlap of the predicted segment area. The predicted results can now be compared to the measured results.

Now the measured values can be compared to the predicted results to validate the 2D measurement of a standard set of pseudo pellets. This will check for any deviations and false rejections that could occur in scanning or will indicate an improper acquisition of the master profile. The results of the measurements can be seen in Table 3.2, the

Table 3.1: Coordinates of Points Used To Calculate Area of $A_4$

| Point | Coordinate | Value |
|---|---|---|
| $P_{21}$ | x | 4.910 |
| | y | 2.222 |
| $P_{31}$ | x | -4.910 |
| | y | 2.223 |
| $P_{23}$ | x | 0.000 |
| | y | -4.788 |

average measured results and the standard deviation of the surface are calculated. These results will then be used to set the thresholds for each scanner, allowing the test surfaces with defective surface deviations to be identified; the desired upper and lower threshold limits will also be identified in the results. The average measured values for each of the segments and the total area of all the segments are as follows:

- Segment $A_1$: 36.973 mm $^2$
- Segment $A_2$: 41.838 mm $^2$
- Segment $A_3$: 41.756 mm $^2$
- Segment Total: 120.567 mm $^2$

It can be seen that the measured values are greater than required, but less than predicted. This is sufficient and due to the manufacturing of the 'viewing windows' not being perfectly accurate. $A_1$ being 7.5% smaller than expected, and $A_2$ and $A_3$ being much bigger than expected; 31.8% and 31.5% respectively. A total of 16.5% more area than expected is being measured. Lastly the lower and upper limit thresholds were chosen to be:

- Scanner 1: 36.800 $mm^2$ - 37.100 $mm^2$
- Scanner 2: 41.500 $mm^2$ - 42.200 $mm^2$
- Scanner 3: 41.200 $mm^2$ - 42.100 $mm^2$

For a pellet to be considered acceptable it must fall within the desired threshold. This results in a total acceptable deviation of 0.3, 0.7 and 0.9 mm $^2$, for each of the cross-sections. A larger measured area will incur a larger deviation based on increase in size. 0.8 - 2 % deviation.

Table 3.2: Measured Results of 2D Scanners 1, 2, and 3

| Scanner Number | Measured Cross-section Values (mm$^2$) | | | | | | | | | | Avg. Value | Std. Deviation | Lower Limit | Upper Limit |
|---|---|---|---|---|---|---|---|---|---|---|---|---|---|---|
| | 1 | 2 | 3 | 4 | 5 | 6 | 7 | 8 | 9 | 10 | | | | |
| 1 | 36.956 | 36.934 | 36.967 | 36.998 | 36.911 | 37.030 | 36.990 | 36.952 | 36.909 | 37.080 | 36.973 | 0.054 | 36.800 | 37.100 |
| 2 | 41.686 | 41.878 | 41.554 | 41.535 | 41.688 | 42.350 | 42.088 | 42.161 | 41.880 | 41.564 | 41.838 | 0.284 | 41.500 | 42.200 |
| 3 | 41.570 | 41.564 | 42.040 | 42.032 | 41.738 | 41.917 | 41.337 | 41.744 | 41.583 | 42.035 | 41.756 | 0.244 | 41.200 | 42.100 |

## 3.2 Surface Integrity

The second of the feature extraction methods to be discussed is the scan of the integrity for each pellet. This process is most important for detecting surface defects, of the three chosen methods of feature extraction. This scan is oriented towards a full scan of the surface of each test piece and will be able to extract surface features and make a pass or fail decision via a single output signal. The accuracy of this signal for detecting the necessary features is unknown and requires that a detection algorithm take place. This seems like a redundant thing to do, however, it is necessary in this case due to the limitations of adapting the equipment to a compatible coding language. The integrity of the pellet, as can be derived from the requirements, can be seen to be of vital importance to the performance of the pellets in a stack and ensuring none are present is of paramount importance to this project. From the literature survey, a few technologies have been found that can be applied to this situation, however, they are mostly contact in nature. The technologies include optical imaging of the pellet and ultrasonic or inductive transmissions through the pellet.

The best technology that was mentioned is the optical method of creating an image of pixels. This differs from the application for the previous feature as it would not rely on shape recognition, but would rely on pixel intensities. In order to be useful the

image should be converted to or captured in gray scale so that the intensities of the pixels are uniformly comparable. It was found that using colour images should only be used when recognition of colour is required. The reasoning behind this application is that a uniform pattern of intensities should indicate a uniform test piece, while an uneven distribution should indicate a lack of test piece integrity. This is a non-contact method for discerning the integrity of the test piece; however, it is limited by lighting and positioning requirements.

### 3.2.1 Chosen Scanning Device: CCD Camera Scanner

A mounted digital camera assembly with a Sony XC-HR70 CCD sensor and LED ring light are used to capture the images of the test piece surface for digital processing (see Figure 3.6).

Figure 3.6: Sony XC-HR70 and LED Ring Light

The intensity of the reflection is measured from the image sensor with a Cognex digital capture card in a PC creating a monochrome digital image having varying degrees of dark to light coloured pixels. In order to detect surface defects, Cognex imaging software is used to create and algorithm that subtracts two images from one another. A standard set of pellets is used to create a set of pictures of verified, i.e., 'good', pellet surfaces. The set of pictures is then compared to each surface that is scanned. Image subtraction is used to subtract the values of each pixel with each of the pellet surface pictures in the standard set. A difference in the pixel intensity will show up

as a lighter shaded pixels on a dark background, where as the subtraction of similar surfaces will result in dark shaded pixels. The lighter shaded pixels will show up in groups where defects are present and can be isolated by comparing neighbouring pixels to look for differences in pixel intensities. After isolating the pixels that represent a defect, a relative area of the defect, the position of the defect from the center of the picture and the number of defects for a scanned surface can be identified.

### 3.2.2 Validation

First the validation consists of a calibration of surface images, with the standard set of calibration pellets. This will be followed by a test of accuracy at measuring defect size and finally setting the minimal thresholds of the filters for 'blob' detection.

The calibration of the cameras consists of recording images and storing them in pixel format picture files, in order to use them in the comparison tool. As was stated, the identified light areas or defects are known as 'blobs' and will be used to assess the accuracy. An example of the subtraction results for a pellet is shown Figure 3.7. The subtraction results can be examined and quantified in terms of pixels and dimensions. This is rationalized because the definition of the CCD sensor, the size of the test pieces, and the size of the camera viewing window are known. Therefore the results can be quantified as a ratio of pixels to the area of the image in $mm^2$. Quantifying the accuracy of the camera system at detecting defects will follow the calibration.

The last step for the validation of the CCD device is to determine and set the blob filter thresholds for each of the scanner algorithms. The thresholds are to be set in the blob recognition part of the algorithm and basically act as a filter for small defects that will be considered negligible. All this means is that any grouping of pixels that occurs and is less than a predetermined amount, will be ignored or not considered a blob at all for the purpose of defect detection. This will be rationalized by relating the probable area of the smallest possible defect that one wishes to detect to the

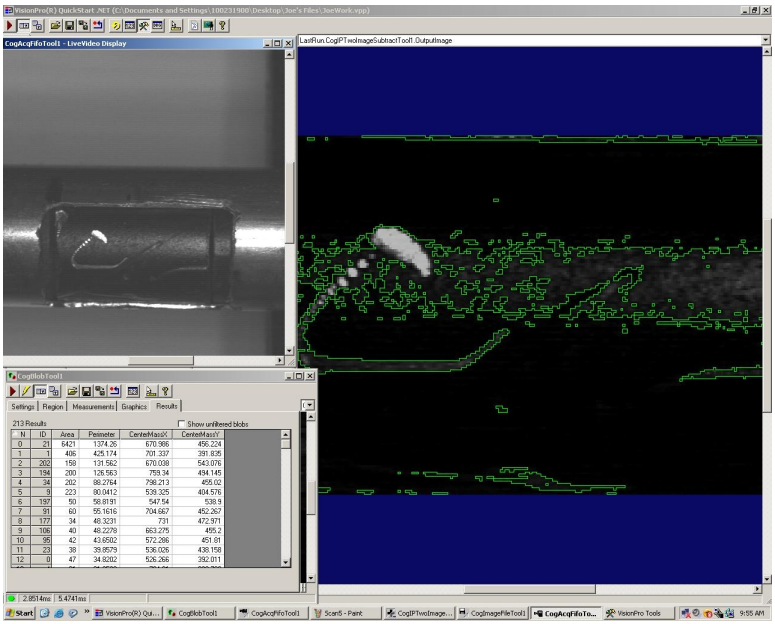

Figure 3.7: Image of Pixel Subtraction

resolution of the image that occurs in said area; in this case resolution is described as pixels/mm$^2$. This will develop a range in which one can fine tune the filter to accept defects of a negligible size. Using an upper and lower limit for the range of possible sized defects, the approximate amount of pixels necessary to achieve the appropriate size of defect can be found. This will also ensure that the filter is not set too high, which could potentially allow a defective pellet to pass. The recorded images are compared to one another using the import from file feature in the camera algorithm, instead of the using the source CCD sensor. This will indicate if the camera algorithm detects defects that appear in the scans of the calibration. Any significant abnormalities should be recorded; the corresponding pellets for any defective scans should be examined to make sure that they fulfill 'good' pellet requirements. The system should be calibrated so that no defects appear between the images of the calibration pellets, using the most minimal of pixel threshold as possible.

### 3.2.3 Validation Results: Surface Integrity Scanning

The calibration of the camera is similar to that of the 2D scanning device as it is employing a method of object comparison, which requires, in this case, acquiring a standard set of images and then the tuning of the filter for the defect size. In between the acquisition of the images and the tuning of the filter, the accuracy of the system has also been evaluated.

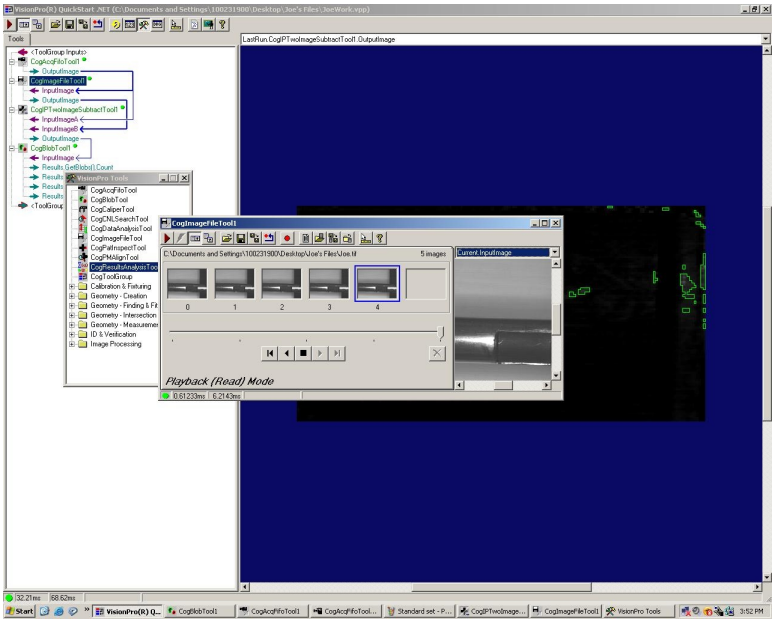


Figure 3.8: Master Set of Standardized Pellets

For the calibration it should be noted that cameras first needs to be positioned to correspond with the 'viewing windows' of the 'pellet chamber'. This should be done so that the test piece is centred in the middle of the image as best as possible. Then the camera view can be set to only look at the area where the pellet will appear and since the scanning structure is rigid, it should not vary during scanning. An example of setting the camera view can be seen in Figures 3.9 and 3.10. After setting the view of each camera, the pixel locations should be recorded for use later in the evaluation of accuracy for each scanner. The master set of standardized surface images, shown in Figure 3.8, is acquired by saving the images of the pellets as data files. The accuracy

of each camera should be validated so that an appropriate range of the thresholds can be found, so that the thresholds are not over or under set with their respective values.

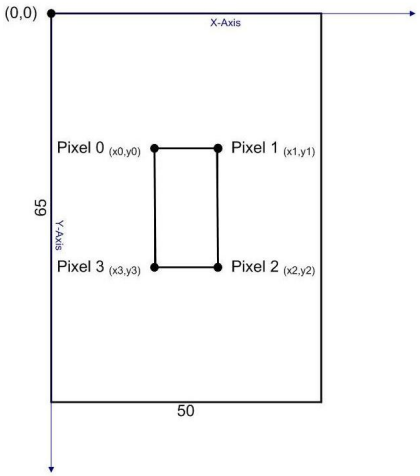


Figure 3.9: Diagram of Theoretical View for Camera 0

The results of the accuracy validation are now presented along with the set thresholds for the system as a whole and then for each respective camera. The size of the defects that can be detected depends on the size of the surface of the test piece being examined, the size of viewing window of the lens, and the degree of definition of the CCD sensor. The current camera setup is using a CCD sensor with a definition of 1,024 x 768 pixels, with a viewing area of approximately 65 mm x 50 mm. This results in an approximate theoretical accuracy of 241.98 pixels/mm$^2$. Since only the test piece will be examined, a good portion of the viewing area is put to waste; it is possible to acquire a smaller viewing area from a more precise lens with a different focal length.

It is also necessary to relate the minimal theoretical size of a defect to the accuracy of the measurement. From the requirements it was said that the approximate size of negligible defects was in most cases below a dimension of 0.5 mm - 0.25 mm. This can be difficult to approximate in terms of area so that estimation can be made of

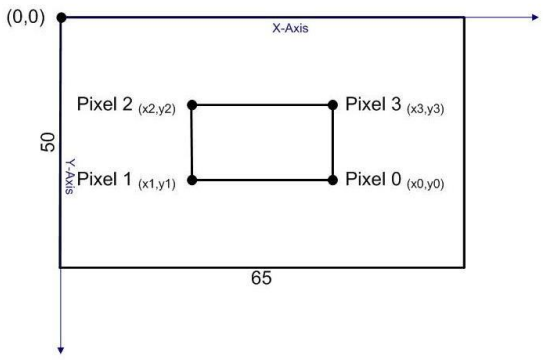


Figure 3.10: Diagram of Theoretical View for Cameras 1 and 2

the apparent area of said defect size. For the purpose of estimation it is assumed that a defect with a corresponding dimension of less than half of the negligible defect size would be appropriate for estimating the negligible defect area size. Thus it was calculated that the lower end of the limit will be for a defect area of approximately 0.04 $mm^2$ and the upper end of the limit will be approximately twice this value at an area of 0.1 $mm^2$. A simple ratio calculation can relate the upper and lower limits of the negligible defect size to the theoretical accuracy of the camera sensor. The reasoning to calculate the upper and lower threshold limits to filter defects can be calculated as

$$LowerPixelThreshold = Min.NegligibleDefectArea \times TheoreticalResolution \tag{3.8}$$

$$UpperPixelThreshold = Max.NegligibleDefectArea \times TheoreticalResolution \tag{3.9}$$

It was calculated that the approximate defect filter threshold of the entire image should be in the range of 9.68 - 24.2 pixels in size, utilizing the most minimal threshold

as possible.

The recorded results for the actual measured accuracy of each camera and the predicted filter thresholds can now be seen in Table 3.3. Using the coordinates of the pixels that make up the 'viewing area', the actual size of each one is calculated using the equation for an irregular polygon. The viewing areas being implemented are irregular polygons for the most part, thus the equation to be used to calculate the area is:

$$A_{ViewingWindow} = \left| \frac{(x_0y_1 - y_0x_1) + (x_1y_2 - y_1x_2) + (x_2y_3 - y_2x_3) + (x_3y_0 - y_3x_0)}{2} \right| \tag{3.10}$$

where xi and yi, i = 0 to 3, are the points defined in Figures 3.9 and 3.10. The results of this equation can be seen in Table 3.3, it was found that the area covered by pixels were as follows:

- Camera 1: 42, 456 pixels
- Camera 2: 22, 604 pixels
- Camera 3: 22, 693 pixels

The results show that there is a minimal variance in the size of 'viewing windows' between Cameras 2 and 3 and a large difference between Camera 1, which is due to the difference in position of the Camera 1 sensor as well as the variance in focal distance. In order to calculate the resolution, the theoretical size of the pellet is used to calculate the approximate area of the 'viewing area'. This is done using the calculations of the segments of the cross-section done in the previous section. From Equation 3.4, the value of c̲an be used to approximate the available diameter of each camera and the length of each pellet is approximately 18 mm. The appropriate corresponding measurements for each segment, to calculate the appropriate area can be seen below:

- $b_1$: 12.216 mm
- $b_2$: 11.782 mm
- $b_3$: 11.782 mm

Thus the value of the viewing area can be calculated and the resolution can be found. The results are seen in Table 3.3. Using the values for resolution the threshold filter limit for each scanner can be approximated and used to set the final filter values. The threshold limits for each scanner are as follows:

- Camera 1: 7.72 pixels - 19.31 pixels
- Camera 2: 4.26 pixels - 10.66 pixels
- Camera 3: 4.28 pixels - 10.70 pixels

Table 3.3: Accuracy Measure of 2D Scanners

| Camera | Coordinate | Pixel 0 | Pixel 1 | Pixel 2 | Pixel 3 | Total Pixels | Resolution | Lower Threshold | Upper Threshold |
|---|---|---|---|---|---|---|---|---|---|
| CCD 1 | x | 441 | 615 | 615 | 441 | 42,456 | 193.080 | 7.72 | 19.31 |
| | y | 420 | 420 | 664 | 664 | | | | |
| CCD 2 | x | 648 | 466 | 463 | 647 | 22,604 | 106.582 | 4.26 | 10.66 |
| | y | 508 | 510 | 386 | 385 | | | | |
| CCD 3 | x | 587 | 405 | 403 | 587 | 22,693 | 107.044 | 4.28 | 10.70 |
| | y | 502 | 503 | 379 | 378 | | | | |

With the threshold limits in mind, the standardized test pieces are then tested to fine tune the filter thresholds. The standardized test pieces should be scanned while slowly incrementing the filter threshold until no or almost no defects appear. This threshold will vary with different lighting and work environment conditions; regardless it should remain within the specified limits for each scanner. For test purposes, the filter values have been set to at 4, 6, and 5 pixels for Cameras 1, 2, and 3 respectively.

Now the algorithm can look for the appropriately sized defects without experiencing the noise caused by negligible imperfections in the test pieces. The images then must be compared to each other, using the import from file feature to check for similarity

between pellets. It is not necessary to record any results here, but to ensure that no sizeable defects are found. It should be seen that the green highlighted blobs will appear, but will be of a small/negligible area. These small or negligible surface imperfections will later be filtered out when the filter thresholds of each camera are set.

## 3.3 Surface Roughness

The last of the three feature extraction methods to be discussed is the surface roughness (Ra) scan for each of the pellets. The importance of this method is to fulfill the functional requirements, maintaining the specifications for pellet performance efficiency and safety. From the literature survey, the applicable technologies for this method included contact probe profilometry and differential refractometry; using specular propagation of both sound and light waves.

The first technology, contact probe profiloemtry, is immediately ruled out because it violates multiple functional requirements. Most importantly it is a contact device; in effect this does slightly alter the surface of the pellet. Also this method is time consuming and is limited to scanning a very small portion of the overall surface. The only applicable technology was the propagation of light waves, using laser light technology. This uses a scan of the surface that works via the same technique as the sound waves; measuring the intensity of the specular reflection. This method is susceptible to interference from other light sources that can usually be suppressed with shielding to eliminate the appropriate spectrums or to eliminate all external light all together. This technology is not affected by a non-contact scenario and does require a gap in order to produce a specular reflection. Laser technology can also achieve a higher frequency than the other technologies due to its shortened wave length and high frequency applicability. This seems to be the most effective technology for measuring

Ra of the test piece in this case.

### 3.3.1 Chosen Scanning Device: Surface Roughness Scanner

A LaserCheck Model 6212C measurement device, which achieves the measurement of surface roughness by aiming a point-laser light at an object so that it has an appropriate angle of reflection off of the scanned surface which is then read by a CCD image sensor (see Figure 3.11). By measuring the amount of diffusion from a specular reflection of a laser light, the average roughness of the surface can be found. The diffusion is measured by using a linear array of CCD sensors. The array measures the intensity of the reflection at different angles, both above and below the angle of specular reflection. The multiple CCD sensors provide voltage readings that are measured by a controller. The measurements, in the form of raw sensor values, are consistent for surfaces of similar surface roughness and thus can be used to achieve an accurate measure. Serial communication is utilized between the sensor controller and a computer/microcontroller. This allows the necessary commands to activate the controller and retrieve the raw data values. The serial communication is set up using a C-code application that is executed using visual studio C++ environment. This application is able to receive the raw data from the controller, adjust the raw value to a calibrated measurement, and distinguish if the surface roughness is within a certain threshold.

### 3.3.2 Validation

The final part of the validation will be to scan for the surface roughness of a test piece, using the laser light profilometry scanner. The specifics of the plan will include an initial calibration of each scanning device, followed by a test for accuracy of the calibration of each sensor head.

The laser scanner supplies a raw digital measurement value from the measurement of

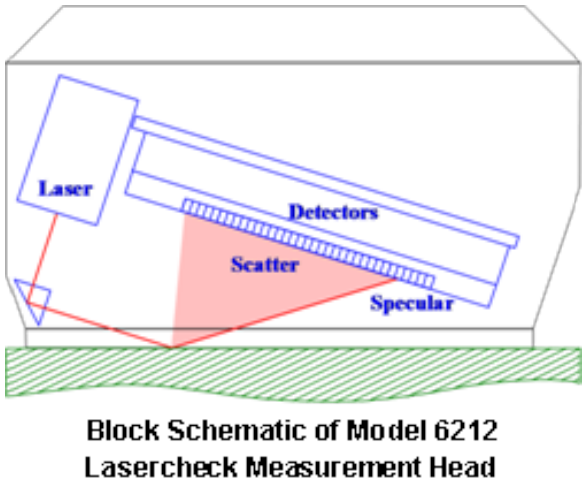


Figure 3.11: The Laser Check 6212C Laser Surface Roughness Scanner [36]

surface roughness of the pellet's surface. This value can be calibrated with surfaces of a known roughness to output an accurate value for surface roughness. This calibration consists of using the raw value measured from the calibration gauge plates to compare them against the verified measurement values for the plates. There are multiple calibrations regions for each scanner because the data received from the scanning head does not respond in a linear fashion to a linear change in surface roughness. The results for the measurements are used to find reliable trend lines for the largest expanse of the given data regions possible. The distinct regions have been indentified and a linear regression was used for each region respectively.

Using the calibration equations for each of the respective ranges, a verification of accuracy on the calibration surfaces is performed. The value received from the device will be fed through the appropriate calibration equations to achieve the final measurement value; to be compared against the known value of the standardized test surfaces. Each of the known values that lie within the region applicable to the corresponding equation and that are relevant to the surface roughness of interest will be recorded. The scans of accuracy will identify the equations that are best suited for the measurement regions of interest.

### 3.3.3 Validation Results: Surface Roughness Scanning

The validation results for this technique evaluated the effectiveness of the point laser profilometry in determining the surface roughness. The raw value of the measurement of diffused reflection are consistent between different surfaces of similar roughness, thus the instrument was first calibrated to conform to a set of roughness gauge plates. After the calibration data was gathered a linear regression was performed to establish calibration equations and was divided into their respective regions for the trend lines of best fit.

For the calibration, the data for each of the three scanners is presented first. This data will be used to find an average raw value of each scanning device for the respective value in the roughness range. The results for the calibration data can be seen in Tables 3.4, 3.5, and 3.6. It can be seen that values were recorded for a range of values from 1 - 125 $\mu$-inches, with each increment approximately doubling the previous one in the range. The results show that Scanner 3 provides raw values that a very different from the other two scanners but that are still in proportion to the change in surface roughness. This shows that scanner results are still useful; however it shows the importance of finding the appropriate calibration equations. Doing things this way, instead of making a comparative measurement only using the raw value from the scanner, is necessary since it easily provides a quantifiable value for the roughness of each surface and not whether or not it compares well to another surface. Another point to note is that for Scanner 1 and 2, is that the measurement values become very close to one another at a roughness over 32 $\mu$-inches. Similarly, Scanner 3 experiences the same effect, but only for the approximate range of 32 - 63 $\mu$-inches.

In order to get an appropriate value of roughness, the calibration data was correlated to the respective values of surface roughness using a linear regression tool. The methodology to accomplish the regression started from the lower end of the regression adding the next incremental value to the regression, until the equation became

Table 3.4: Calibration of Ra Scanner No.1

| Calibration Value ($\mu$-inches) | Calibration Value ($\mu$m) | Measured Value ($\mu$-inches) | | | | | | | | | | Average Measured Result ($\mu$-inches) |
|---|---|---|---|---|---|---|---|---|---|---|---|---|
| | | 1 | 2 | 3 | 4 | 5 | 6 | 7 | 8 | 9 | 10 | |
| 1 | 0.025 | 0.2108 | 0.211 | 0.211 | 0.2114 | 0.2114 | 0.2112 | 0.2112 | 0.211 | 0.2112 | 0.211 | 0.21112 |
| 2 | 0.05 | 0.4612 | 0.4612 | 0.462 | 0.462 | 0.4628 | 0.4628 | 0.4628 | 0.4628 | 0.4628 | 0.4636 | 0.4624 |
| 4 | 0.1 | 0.668 | 0.6688 | 0.668 | 0.6688 | 0.668 | 0.6672 | 0.668 | 0.6688 | 0.6696 | 0.6688 | 0.6684 |
| 8 | 0.2 | 1.4687 | 1.4656 | 1.4672 | 1.4704 | 1.472 | 1.4704 | 1.4687 | 1.4672 | 1.4656 | 1.4656 | 1.46814 |
| 16 | 0.4 | 4.0608 | 4.0656 | 4.064 | 4.0544 | 4.0528 | 4.0512 | 4.0512 | 4.0496 | 4.056 | 4.0576 | 4.05632 |
| 32 | 0.8 | 10.0128 | 10.0224 | 10.0208 | 10.008 | 9.956 | 9.9928 | 9.9888 | 9.9912 | 9.9712 | 9.996 | 9.996 |
| 63 | 1.6 | 10.32 | 10.3048 | 10.2903 | 10.3096 | 10.3232 | 10.3135 | 10.3408 | 10.2864 | 10.3144 | 10.3208 | 10.31238 |
| 125 | 3.2 | 18.1312 | 18.152 | 18.1232 | 18.192 | 18.1551 | 18.2056 | 18.1744 | 18.1888 | 18.1736 | 18.1 | 18.15959 |

Table 3.5: Calibration of Ra Scanner No.2

| Calibration Value ($\mu$-inchhes) | Calibration Value ($\mu$m) | Measured Value ($\mu$-inchhes) | | | | | | | | | | Average Measured Result ($\mu$-inches) |
|---|---|---|---|---|---|---|---|---|---|---|---|---|
| | | 1 | 2 | 3 | 4 | 5 | 6 | 7 | 8 | 9 | 10 | |
| 1 | 0.025 | 0.3495 | 0.3492 | 0.3492 | 0.3495 | 0.3492 | 0.3492 | 0.3495 | 0.35 | 0.3495 | 0.3495 | 0.34943 |
| 2 | 0.05 | 0.5299 | 0.5296 | 0.5299 | 0.5308 | 0.5304 | 0.5296 | 0.5296 | 0.5304 | 0.5299 | 0.5312 | 0.53013 |
| 4 | 0.1 | 0.7176 | 0.7176 | 0.7176 | 0.7184 | 0.7192 | 0.7192 | 0.72 | 0.72 | 0.7192 | 0.72 | 0.71888 |
| 8 | 0.2 | 1.4912 | 1.4912 | 1.4895 | 1.4895 | 1.4895 | 1.4912 | 1.4895 | 1.4912 | 1.4928 | 1.4928 | 1.49084 |
| 16 | 0.4 | 3.6928 | 3.6944 | 3.6944 | 3.688 | 3.6816 | 3.6784 | 3.68 | 3.6816 | 3.6848 | 3.6832 | 3.68592 |
| 32 | 0.8 | 9.6639 | 9.6496 | 9.6544 | 9.6592 | 9.6496 | 9.6544 | 9.656 | 9.6544 | 9.656 | 9.6544 | 9.65519 |
| 63 | 1.6 | 11.408 | 11.3808 | 11.3928 | 11.4032 | 11.3784 | 11.384 | 11.404 | 11.4296 | 11.3896 | 11.3823 | 11.39527 |
| 125 | 3.2 | 13.8 | 13.8784 | 13.8336 | 13.8608 | 13.8632 | 13.8488 | 13.8552 | 13.852 | 13.8584 | 13.8848 | 13.85352 |

unusable. This was quickly done using a visual representation of the plotted values and the curves based on the equations generated in the linear regression. Each of the equations thus represents each of the distinct surface roughness regions. The equations are represented as piecewise functions, indicating the scanner, scanning regions and value ranges:

$$Scanner1 \begin{cases} Region1(1-32) & = 0.0107x^4 - 0.1033x^3 - 0.3683x^2 + 6.5472x - 0.5067 \\ Region2(32-63) & = 97.983x - 947.44 \\ Region3(63-125) & = 7.9009x - 18.477 \end{cases} \tag{3.11}$$

$$Scanner2 \begin{cases} Region1(1-8) & = -16.942x^3 + 40.781x^2 - 20.368x + 3.8604 \\ Region2(8-125) & = 0.1433x^3 - 2.0899x^2 + 10.774x - 3.4467 \\ Region3(32-125) & = 1.9058x^2 - 22.692x + 73.72 \end{cases} \tag{3.12}$$

Table 3.6: Calibration of Ra Scanner No.3

| Calibration Value ($\mu$-inches) | Calibration Value ($\mu$m) | Measured Value ($\mu$-inches) | | | | | | | | | | Average Measured Result ($\mu$-inches) |
|---|---|---|---|---|---|---|---|---|---|---|---|---|
| | | 1 | 2 | 3 | 4 | 5 | 6 | 7 | 8 | 9 | 10 | |
| 1 | 0.025 | 3.3349 | 3.3411 | 3.3442 | 3.338 | 3.3473 | 3.3596 | 3.3504 | 3.3627 | 3.3658 | 3.375 | 3.3519 |
| 2 | 0.05 | 4.737 | 4.7339 | 4.7339 | 4.7464 | 4.7464 | 4.7495 | 4.7557 | 4.762 | 4.762 | 4.762 | 4.74888 |
| 4 | 0.1 | 6.1591 | 6.1628 | 6.1722 | 6.1816 | 6.1909 | 6.2003 | 6.2096 | 6.2096 | 6.2128 | 6.2128 | 6.19117 |
| 8 | 0.2 | 9.2516 | 9.2704 | 9.2641 | 9.2516 | 9.2516 | 9.2454 | 9.2454 | 9.2454 | 9.2516 | 9.2579 | 9.2535 |
| 16 | 0.4 | 15.4292 | 15.423 | 15.4729 | 15.448 | 15.488 | 15.4417 | 15.448 | 15.4729 | 15.4667 | 15.4542 | 15.45446 |
| 32 | 0.8 | 75.7866 | 76.1463 | 76.0948 | 76.1205 | 75.9149 | 76.4554 | 77.0243 | 76.6103 | 76.7912 | 76.3523 | 76.32966 |
| 63 | 1.6 | 81.0963 | 79.5255 | 80.7084 | 79.7108 | 79.8566 | 78.9579 | 81.7409 | 79.0764 | 79.8036 | 79.3272 | 79.98036 |
| 125 | 3.2 | 209.7802 | 205.406 | 207.3439 | 204.2113 | 209.8733 | 204.4637 | 208.5253 | 212.9354 | 209.0128 | 212.7711 | 208.4323 |

$$Scanner3 \begin{cases} Region1(1-16) & = -0.0057x^3 + 0.1652x^2 - 0.1558x - 0.1869 \\ Region2(16-32) & = 0.2628x + 11.938 \\ Region3(32-63) & = 8.4915x - 616.16 \\ Region4(63-125) & = 0.4827x + 24.396 \end{cases} \tag{3.13}$$

Examining the results can reveal some points of interest, which show some inconsistencies between the scanners; all of which can be corrected. Each of the equations for the scanners will be examined with these points in mind. Beginning with Scanner 1, it can be seen that Region 1 is described by a complex equation, while the remaining regions are described in a linear fashion. The value range of Regions 1 and 2 will be chosen to achieve the measurement values for accuracy of the roughness, since the upper and lower limit is in the maximum and minimum of the regions, respectively.

Next, Scanner 2 was examined, it was seen that there was no linear response to the data and that complex equations were necessary to describe all of the calibration regions. Differing from the Scanner 1, it was found that two regions overlap in almost their entirety. The regions were Region 2 and 3, which begin and 8 and 16 $\mu$-inches and both extend to 125 $\mu$-inches. The two equations will be compared to each other for the accuracy measurements of surface roughness.

The last regression was for Scanner 3, where all the regions found responded in a linear fashion, except for the first region. Another point of interest was that the final scanner needed four regions to describe the entire range of roughness values. This is seemingly

due to the fact that the scanner achieves a different range of raw values from the other two scanners; which achieve very similar raw values. Similarly to the Scanner 1 results, there was an overlap in the value of roughness of interest and thus the equations for Regions 1, 2, 3, and 4 are all used to evaluate the accuracy. By evaluating all the possible and relevant regions for accuracy, the most suitable calibration equation(s) can be identified and used to calculate apparent surface roughness, from the received scanner raw value results.

To recall from Chapter 1, the measurement region of interest is 0.800 $\mu$m; which is equivalent to 32 $\mu$-inches. Knowing this, the appropriate calibration equations are used to calculate surface roughness, given the raw value from the specified scanner. The results are used to calculate the error for the calibration equations, as well as the standard deviation for each scanner. A high value for error will show that the calibration equation is not very good for use at calculating the surface roughness. This can be acceptable if the result is repeatable and if it is the equation of best fit. Similarly a high standard deviation is unacceptable since it indicates an unstable scan in that measurement region, this cannot be adjusted for.

The following will detail the analysis of the accuracy results for each of the three scanners. It can be seen from the results that Scanner 1 has the best response to the calibration surfaces, followed by Scanner 3 and Scanner 2. Starting with the results for the accuracy of Scanner 1, they can be found in Table 3.7. The largest difference seen in Region 2 is approximately 0.3 $\mu$-inches over the entire range resulting in 0.94 - 1.87 % error. The next region has a difference range of 0.4 - 2 $\mu$-inches over the range resulting in 1.25 - 3.17 % error. Next the results for the accuracy of Scanner 2 can be found in Table 3.8. The differences for Region 2 were found to be in the range of 0.3 - 8 $\mu$-inches resulting in a 1.87 - 21 % error. Similarly for Region 3, a slight increase in the range was found, it was between 2 - 8 $\mu$-inches resulting in a 10 - 21 % error. This is a very inaccurate degree of percentage error, but if necessary can

calculate for offset by distributing the error of the desired region over the respective ranges of values. The final results for the accuracy of the Ra scanners is for Scanner 3, they are found in Table 3.9. Unlike the other scanners there were four calibration equations used to correlate the measured values to the known ones. All of the regions were tested for accuracy; however for the purposes of analysis only Regions 2 and 3 will be evaluated. The results for Region 2 show that there was a difference of 0.45 - 0.07 $\mu$-inches and the results for Region 3 show that there was a difference of 2.2 - 5.1 $\mu$-inches. This resulted in a 3 - 0.22 % and 6.9 - 8.1 % error, respectively.

The chosen equations based on the accuracy results and relevant percentage errors are as follows:

1. Scanner 1(Region 1): $\text{Ra} = 0.0107x^4 - 0.1033x^3 - 0.3683x^2 + 6.5472x - 0.5067$
2. Scanner 2(Region 2): $\text{Ra} = 0.1433x^3 - 2.0899x^2 + 10.774x - 3.4467$
3. Scanner 3(Region 2): $\text{Ra} = 0.2628x - 11.938$

Table 3.7: Accuracy Results of Ra Scanner No.1

| Reference Ra Value ($\mu$-inches) | Measured Ra Value ($\mu$-inches) | | | | | | | | | | Standard Deviation |
|---|---|---|---|---|---|---|---|---|---|---|---|
| | 1 | 2 | 3 | 4 | 5 | 6 | 7 | 8 | 9 | 10 | |
| 16(Region 1) | 15.68111 | 15.69115 | 15.69615 | 15.69115 | 15.69365 | 15.69365 | 15.68864 | 15.69365 | 15.69365 | 15.69365 | 0.00422805 |
| 32(Region 1) | 31.74756 | 31.85289 | 31.78261 | 31.67764 | 31.62536 | 31.6602 | 31.6951 | 31.79796 | 31.73006 | 31.71257 | 0.06900292 |
| 32(Region 2) | 31.60614 | 32.54677 | 31.91968 | 30.97904 | 30.50873 | 30.82227 | 31.13582 | 32.05686 | 31.44936 | 31.29259 | 0.61807523 |
| 63(Region 2) | 65.04499 | 65.07028 | 64.81745 | 65.15877 | 65.09477 | 65.1082 | 65.00628 | 64.9565 | 64.93122 | 64.98179 | 0.10015511 |

Table 3.8: Accuracy Results of Ra Scanner No.2

| Reference Ra Value ($\mu$-inches) | Measured Ra Value ($\mu$-inches) | | | | | | | | | | Standard Deviation |
|---|---|---|---|---|---|---|---|---|---|---|---|
| | 1 | 2 | 3 | 4 | 5 | 6 | 7 | 8 | 9 | 10 | |
| 16(Region 2) | 15.25959 | 15.25794 | 15.25794 | 15.25794 | 15.25959 | 15.25794 | 15.25628 | 15.25959 | 15.25794 | 15.25794 | 0.00104578 |
| 16(Region 3) | 14.40369 | 14.41637 | 14.41637 | 14.41637 | 14.40369 | 14.41637 | 14.42906 | 14.40369 | 14.41637 | 14.41637 | 0.00802092 |
| 32(Region 2) | 40.5953 | 40.63594 | 40.63594 | 40.575 | 40.75812 | 40.79894 | 40.67662 | 40.575 | 40.63594 | 40.5953 | 0.07628769 |
| 32(Region 3) | 39.92229 | 39.97363 | 39.97363 | 39.89663 | 40.12791 | 40.17941 | 40.02502 | 39.89663 | 39.97363 | 39.92229 | 0.09633613 |
| 63(Region 2) | 53.44887 | 53.32676 | 53.28612 | 53.35387 | 52.0429 | 53.1914 | 53.31321 | 52.9217 | 53.20492 | 53.21845 | 0.15455558 |
| 63(Region 3) | 55.31181 | 55.17255 | 55.12618 | 55.20348 | 54.8484 | 55.01806 | 55.15709 | 54.7098 | 55.0335 | 55.04894 | 0.17650278 |

## 3.4 Summary

The design of the automated scanning system is outlined in the design report [1] based on the background research conducted on NDT part scanning technologies. The

Table 3.9: Accuracy Results of Ra Scanner No.3

| Reference Ra Value ($\mu$-inchees) | Measured Ra Value ($\mu$-inches) | | | | | | | | | | Standard Deviation |
|---|---|---|---|---|---|---|---|---|---|---|---|
| | 1 | 2 | 3 | 4 | 5 | 6 | 7 | 8 | 9 | 10 | |
| 16(Region 1) | 19.73865 | 19.76776 | 19.78673 | 19.73533 | 19.76134 | 19.75494 | 19.78357 | 19.69502 | 19.677779 | 19.67433 | 0.04177 |
| 16(Region 2) | 16.55529 | 16.57003 | 16.57989 | 16.55364 | 16.56675 | 16.56349 | 16.57823 | 16.53395 | 16.52575 | 16.52412 | 0.02068032 |
| 32(Region 2) | 31.92896 | 31.84124 | 31.90194 | 31.76048 | 31.6197 | 31.78736 | 31.67326 | 31.50619 | 31.58627 | 31.70006 | 0.13855249 |
| 32(Region 3) | 29.78076 | 26.9463 | 28.90784 | 24.33686 | 19.78797 | 25.20554 | 21.51853 | 16.12049 | 18.70785 | 22.38467 | 4.47685866 |
| 63(Region 3) | 57.89527 | 62.84412 | 66.57104 | 61.60436 | 70.99171 | 61.71729 | 71.90115 | 61.71729 | 69.74261 | 80.80449 | 6.84386391 |
| 63(Region 4) | 62.71273 | 62.99404 | 63.2059 | 62.92357 | 63.45719 | 62.92999 | 63.50889 | 62.92999 | 63.38619 | 64.015 | 0.38903999 |

research covered topics relevant to scanning the surfaces of ceramics and cylinders and high-speed non-contact NDT techniques. Due to the fact that $UO_2$ is a specialized material, it was found that many NDT scanning techniques and technologies were not applicable to this application. Most traditional scanning techniques will not respond well to ceramic materials or to uranium. The properties of the ceramic uranium pellets are such that they do not respond well to inductive, acoustic, or irradiative methods of default detection, due to the material's low magnetic properties and its high density.

It was determined that to satisfy the requirements, optical methods should be used for detection of pellet defects. It is assumed that an optical method of scanning will consist of a light source directed at the surface of a uranium pellet, coupled with a sensor to measure the intensity of the light reflected. With current technology, an opportunity exists to capture digital images and process them at high speeds. An important note is that the term 'digital image' will not be specifically limited to a picture, but instead include any digital signal obtained from an image sensor that can be recorded and processed.

Three different scanning techniques were investigated in detail. Each of these techniques is used to examine a different specification or defect, while also achieving redundancy in comparative scanning and measurements. It was found that there should be inspection stages based on evaluating: surface profile, surface integrity, and surface roughness. The first stage uses a 2D laser scan of the surface profile. The second stage uses digital imaging technology to scan the surface for any defects. The last stage of inspection uses a laser profilometer to find the variance in the surface

roughness (Ra) with a high degree of accuracy.

# Chapter 4

# Defect Testing Results for The Automated System

This chapter presents the testing plan and results of the proposed scanning system at detecting the identified defects. Due to the confidential nature of the system design, only the test results will be presented. For details about the system design, the reader is referred to [1]. Since each scanner functions differently, it is inherent that one scanner will be better at detecting certain defects than another scanner. The predicted results will be stated based on each scan type, in relation to the types of defects to be detected. The results of the testing will be determined by using six sets of defective pseudo pellets to evaluate the effectiveness of each scanner at detecting the specified defect. Each type of defect will be discussed to indentify specifically what is being sought after when detecting that defect. For each type of defect there are three pseudo pellets that make up the set, they represent an example of deviation in the type of defect that is being analyzed.

This is only a starting point to qualify the system at scanning defective pellets, so that it is deemed to be at a level where it can be used to examine actual fuel pellets. The system will be qualified in detecting defects, by way of a test plan that has been

followed. The test plan will indicate how the scans are being conducted with the pseudo pellets and will indicate what observations are to be recorded. The recorded results will then be presented for each identified type of defect. Only the results for the set of defective pellets will be presented in the results section. The results will be analyzed to identify which type of scans can detect which type of defect; this will then be compared to the expected results.

It is necessary to predict the type of scanners that will detect the various types of defects. This is to provide a baseline of what to expect and can be used to determine if there are any discrepancies in the scans. Since the accuracy of each type of scanner has been determined, anything out of the ordinary must be traced back to the root cause. This will make it possible to detect scanners that miss the appropriate defects and any scanners that show unexpected anomalous measured values.

The types of defects that are detected by each of the scanners are as follows: The 2D scan measures the difference in the shape of the cross-section via calculating the area. This would indicate that this type of scan will be best suited towards detecting any defects that vary the shape of the cross-section. So defects that create a low spot or high spot along the circumference of the pellet will show up well. This type of scanner will be excellent at detecting all types of defects except for wheel marks and non-cleanups; which it may have difficulty with.

The CCD scan measures the difference in surface integrity between a known set of 'good' pellets and the 'test piece' to be scanned. A CCD scan is able to detect all types of surface imperfections that are being scanned for, with the exception of surface roughness. The other two type of scans serve as redundancies and provide extra reassurance that pellets are defect free.

In this system, the CCD has not been orchestrated to scan for surface roughness or perhaps some wheel marks or non-cleanups. A separate set of sensors has been applied to do this in the form of the laser profilometry scan. The Ra or laser profilometry scan

will measure the height differential in the surface variation. Thus any continual change in surface variation may be detectable by means of laser surface profilometry. This type of scan is best suited at detecting surface roughness and can also detect wheel marks and non-cleanups. It should be noted that all the scans can show potential at detecting surface roughness, but are more difficult to implement without this type of arrangement. This type of scan may also show potential at detecting crack defects if they lie in the same orientation of the Ra scan.

## 4.1 Pseudo Defective Pellets

The following will outline what the scanners will be using in order to accomplish the defect testing procedures. In order to perform the defect testing effectiveness, six sets of defective pseudo pellets have been created. It was necessary to refer to the defective pellet pictures seen in Section 1.3.2, in order to correctly identify the type of features present in each type of defect. The pseudo defective pellets can be seen pictured in Figures 4.1 to 4.6. Each type of defect will be described and each of the three pellets will be presented. It may be noticed that some of the defects are difficult to see in the pictures, the pictures are only meant to serve as a guide to number each of the tested pellets for the purposes of presenting the results. Upon close visual and tactile examination all the defects can be seen to be present. Also the defects are of a small size to best evaluate the effectiveness of the system at detecting defects until they are declared as undetectable or negligible. One last note is that each set of defective pellets have been inscribed with roman numerals on the end of each pellet to indicate its number.

To reiterate the types of defects are as follows:

1. Chips (see Figure 4.1)

2. Cracks and End Cracks (see Figure 4.2)

3. End Squares (see Figure 4.3)

4. Inclusions and Pits (see Figure 4.4)

5. Wheel Marks (see Figure 4.5)

6. Non-Cleanups (see Figure 4.6)

### 4.1.1 Chip Defect (Defect 1)

The first type of defect to be discussed will be 'chip' or 'end-chip' defects, which have been shown to occur at the ends of the pellets; usually occurring at one end or the other. These chips can be large or occur in smaller form around the circumference of the end of the pellet. This type of defect will be indicated by a continuous chipping that would have occurred in the grinding process. The pseudo pellets shown in Figure 4.1 have the same types of features, but have been made smaller scale. It can be seen that Pellet 1 has the large end chip type defect at one end of the pellet. Pellet 2 can be seen to have one small type defect, which may be more difficult to detect. The last type of defect was having smaller end chipping around the circumference of the end of the pellet, pictured in the Pellet 3. This type of defect will present itself in the scan of surface shape, as well as the CCD scan for surface integrity.

### 4.1.2 Crack Defect (Defect 2)

Next, the type of 'crack' defects that have be shown to present themselves will be discussed. For this defect the pellets show the occurrence of end cracks, longitudinal cracks and horizontal ones. These types of cracks occur more towards the end of the pellets, but can occur at any point on the pellets surface with no particular orientation. These defects will typically have a crevasse feature that extends, from a few millimetres to multiple millimetres, in a fracturing pattern of orientation. This type of defect is identified by a cracking in the surface of the pellet caused in the

Figure 4.1: Pseudo Test Pellets with "End-Chip" Defects: Pellet 1 (Upper Left), Pellet 2 (Upper Right), Pellet 3 (Bottom)

sintering or grinding process. The pseudo defect pellets shown in Figure 4.2 have the same types of features, separated into the distinct variance of orientation. It can be seen that Pellet 1 has the longitudinal type defect occurring at the end of the pellet. Pellet 2 can be seen to have a horizontal type defect near one end and Pellet 3 has a horizontal crack defect near the centre of the pellet. This type of defect is detected with the scan for surface shape and surface integrity, there is also a potential to recognize this type of defect with the Ra scan.

### 4.1.3 End Square Defect (Defect 3)

The third type of defect is the 'end square', which differs from the 'end chip' type defect. Pellets with the defect show that there is a distinct variation in the end shape of the pellet. This type of defect occurs on one end of the pellet, due to malformations during the sintering process, and will vary in size and severity. The pseudo defect

Figure 4.2: Pseudo Test Pellets with "Crack" Defects: Pellet 1 (Upper Left), Pellet 2 (Upper Right), Pellet 3 (Bottom)

pellets that are shown in Figure 4.3 have the same types of features, but have been made smaller scale. It can be seen that the Pellet 1 has an end square that is somewhat uneven, shallow, and it drifts to the side. Pellet 2 has a deep and uneven end square defect. Lastly, Pellet 3 is seen to have a large glancing end square defect. This type of defect will be most accurately identified with the scan for surface shape. Also there is potential for the surface integrity scan or Ra scan to notice a void in the surface being scanned.

### 4.1.4 Inclusion and Pit Defects (Defect 4)

The next type of defect that is discussed are 'inclusions and pits', which present themselves in two variations. The inclusions in particular will be indicated as a colour variation in the surface material or a blemish on the surface, appearing as a protrusion, indentation, surface discolouration, or a combination of the three. The

Figure 4.3: Pseudo Test Pellets with "End Square" Defects: Pellet 1 (Upper Left), Pellet 2 (Upper Right), Pellet 3 (Bottom)

pit will be indicated by a dimple in the pellet surface, appearing as a crater with varying size. The pseudo defective pellets shown in Figure 4.4 will exhibit two 'pit' type defects and one 'inclusion' type defect. It can be seen that Pellet 1 is a very small pit type defect. Pellet 2 exhibits multiple inclusions along the surface of the pellet; centralized in two distinct spots. Pellet 3 contains a single deeper pit type defect centralize in the middle of the surface of the pellet. This type of defect will be most easily discovered in the CCD scan since its occurrence can be very small and the surface shape scan would potentially have to be triggered at an exact instant in order to achieve the appropriate cross-section. It is unlikely that the Ra scan will prove at all useful at detecting pits or inclusions.

Figure 4.4: Pseudo Test Pellets with "Inclusion and Pit" Defects: Pellet 1 (Upper Left), Pellet 2 (Upper Right), Pellet 3 (Bottom)

### 4.1.5 Wheel Mark Defect (Defect 5)

The fifth type of defect that was exhibited in the requirements was the 'wheel-mark' type of defect. This defect is characteristic of a flat spot on the surface of the pellet that has occurred due to a stall of some sorts of the pellet while being ground in the grinding process. The pseudo defect pellets in Figure 4.5 show a 'wheel mark' via a flat spot on the pellet surface. Beginning with Pellet 1, a thin long area can be seen to exhibit the wheel mark characteristic. Next, Pellet 2 shows a wide defective area oriented towards one end of the pellet. Lastly, Pellet 3 shows a mid-ranged size defect that occurs near one end of the pellet. This type of defect will be noticed by all types of scanners; the Ra scanner may have difficulty if the wheel mark does not appear along the scan path. This defect type will appear in either the scan for surface shape or surface integrity.

Figure 4.5: Pseudo Test Pellets with "Wheel Mark" Defects: Pellet 1 (Upper Left), Pellet 2 (Upper Right), Pellet 3 (Bottom)

### 4.1.6 Non-Cleannup Defect (Defect 6)

The final defect to be discussed is the type of defects that present themselves as a non-cleanup type of defect. The non-cleanup defect is mostly generated when there is a portion of the pellet that has not had its surface ground symmetrically around the circumference of the pellet or not ground in a spot at all. The pseudo defective pellets shown in Figure 4.6 present a non-cleanup defect in the form a rough or uneven surface uncharacteristic to the normal surface of the pseudo pellet. This is a somewhat difficult defect to emulate since the beginning product for the pseudo pellet has a uniform surface. This being the case, the set of pseudo defective pellets is not very distinctive from one another, having varying degrees of size of defective surface areas. The non-cleanup is similar to the wheel mark except the surface shape could be very close to an acceptable standard and hard to detect with the scan for surface shape. The scan of surface integrity and the Ra scan should provide enough

redundancy to accurately detect this type of defect.

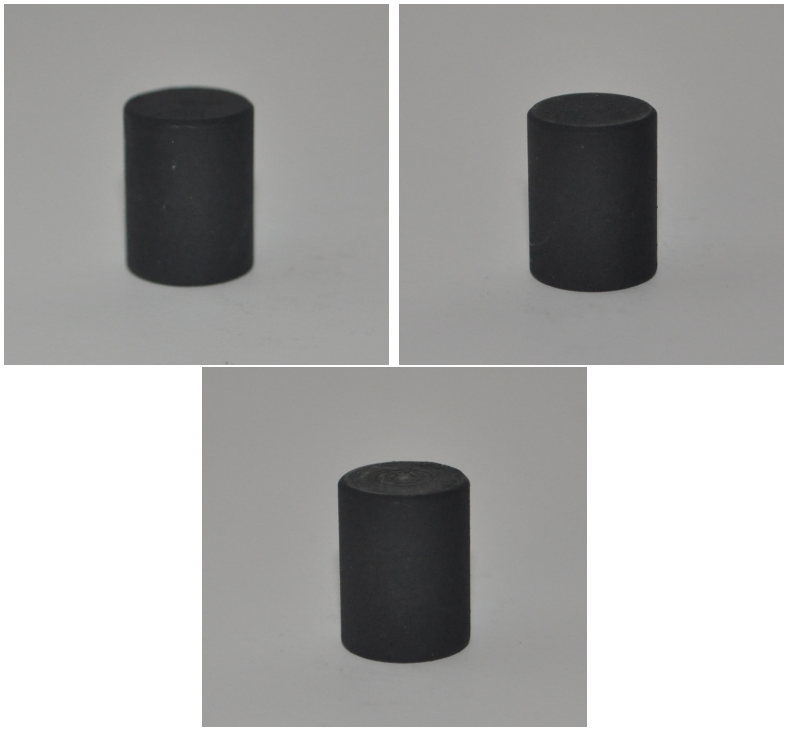

Figure 4.6: Pseudo Test Pellets with "Non-Cleanup" Defects: Pellet 1 (Upper Left), Pellet 2 (Upper Right), Pellet 3 (Bottom)

## 4.2 Defect Test Plan

Now that the predicted results for each scanner and the types of defects have been discussed in detail the test plan can be outlined. The test plan will use each scanner to measure each kind of defect pellet. The scans for each type of defect will be separated by un-altered pseudo pellets with a metallic surface. The results for defect scans will be presented only without the average scan value or other acquired values from the scanners. The results will be presented in the appropriate measurement values for each of the respective scanners: $mm^2$ for the 2D scanner, pixels for the CCD sensors, and $\mu$m for the surface roughness scanners.

For these tests, each of the defective pellets should be indicated as defective by at least one of the scanners, as it is not necessary for all of the scanners to recognize a

defect of the pellet surface. This is due to the position and orientation of the defect on the pellet surface or the nature of the defect; some scanners are inherently good at detecting certain types of defects while others are not. From these tests it is expected that the 2D scanner will detect most of the defects except non-cleanup defects (Defect 6), since this type of defect will minimally change the surface shape, and inclusions (Defect 4) that have been ground flush with the surface. The CCD scanner will detect all the defects with the exception of surface roughness defects. Finally the Ra scanner, which is designed solely for the purpose of detecting surface roughness, will have the ability to detect defects that inherently change the surface roughness of the pellet. The Ra scanner may be able to detect Defects 3, 5, and 6, and whether or not the surface roughness is acceptable. There is also a possibility for the surface roughness scanner to detect Defect 2 as long as it passes through the scanning area.

The testing will present the acquired results from scanning each type of defect and analyze the results to indicate which defect the respective scanners do detect. For this test the pellets were scanned in groups of threes with non-pseudo pellets used as spacers to indicate which data is not from the pseudo defective pellets. The layout of the defective pellets to be tested and the pellets to be used as spacers can be seen in Figure 4.7. To test Defect 1, three pellets were scanned and spaced apart so that no two pellets were being scanned by the same type of device. The loading and the unloading of the pellets was done manually and the metallic pellets were re-used as they exited the system, whereas the defect pellets were replaced with the next type of defect. Defects 2 through 6 were scanned in the same fashion, and all the results were tabulated and analyzed to present the measurements achieved in the defective regions only. This provides a benchmark for expected defective scan results and a visual representation of example defects to go along with it. The measured values for the defects reveal what scanners can detect what defects, which can then be compared to the expected results.

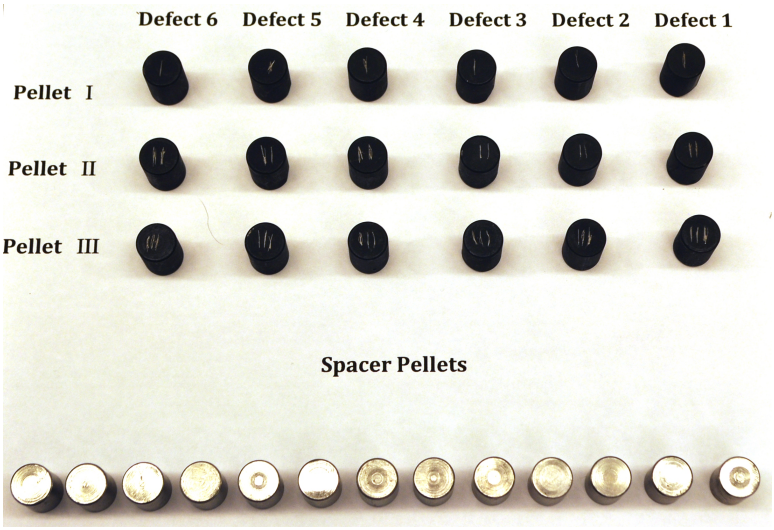


Figure 4.7: Pseudo Test Pellets with Defects Queued Up for Testing

## 4.3 Defect Test Results

Following the test plan, the results of the scans from passing the defective pellets through the system were recorded. These test results will be used to indicate if the identified defect can be recognized by any of the three scanners. The scanners that can detect each type of defect will be indentified and the results will be analyzed. This will reveal how the measurement results can be affected by each kind of defect. It may be noticed that in some scans no defective results are present, this can occur for a few reasons. One reason is that no defect passed through the viewing window of the scanner that returned no defective measurements, since it is probable that the defect instead passed through the viewing window of one of the other scanners. Also, it can be possible that one type of scanner does not have the ability to detect certain defects. This will also be covered in the analysis of each scanner for each of the six defects. The scanner results are also presented and will be briefly discussed in relation to each type of scanner.

Each scanner records many scan results and as such will be too confusing to present a mass of results. Instead the results will be presented in a manner that will best highlight the defect detection capabilities of each of the three types of scanners. This

involves analyzing the results to present the correlating scanned values, for the presence of a defective or acceptable surface. In the case of a defective surface, it will be indicated with an asterix and an example of a defective measurement will be presented. In the case of an acceptable surface an average measurement value will be presented. Each set of defect results will be presented in a table showing the results for each of the nine scanning windows separately, for each of the three pellets of each type of defect. From the results it can be seen that an acceptable surface for the 2D scan is around 36.67 - 38.35 $mm^2$ for scanner 1 and 41.04 - 42.48 $mm^2$ for scanners 2 and 3. For the CCD scan an acceptable measured value for a given surface is below approximately 22 pixels. For the Ra scan an acceptable surface measures between 20 $\mu$-inches and 37 $\mu$-inches. It must be noted that the results for an acceptable surface do not exactly coincide with specifications of production, but are used as a benchmark for the testing of pseudo pellets. These results are, for the most part, achieving the predicted values of a theoretically perfect surface, as was seen in the validation; found in Chapter 3.

### 4.3.1 Test Results: Defect 1

The first type of defect that was tested was the pseudo pellets with the simulated "chip" or "end-chip" type of defect. This type of defect had to be replicated; it was not possible to chip the ends of the pseudo pellets. From the results, seen in Table 4.1, it is shown that each type of scanner is able to detect this type of defect to some degree. The 2D scanner was able to detect both small and large chip defects, that create a 2 - 5 $mm^2$ difference, that pass through the viewing window; this was within a strict threshold, especially for the smaller defects. The defects are also very apparent in the CCD scanner results, both large and small areas of pixels; some as large as 3,000 pixels and some as small as 200 pixels, show up in the subtraction algorithm. Lastly, the Ra scanner is able to detect sufficiently large end chip defects that are able to

pass through the scanning area. This defect appears in the surface roughness results as an abnormally low value for surface roughness, as low as 9 $\mu$-inches, which was not expected intially because a defect such of this was thought to be out of scanning range. This discovery can be considered for the remainder of the results now.

Table 4.1: Test Results for Defect 1: Chips

| Type of Scanner | 2D Scanner ($mm^2$) | | | CCD Scanner (pixels) | | | Ra Scanner($\mu$-inches) | | |
|---|---|---|---|---|---|---|---|---|---|
| Number of Scanner | scanner 1 | scanner 2 | scanner 3 | scanner 1 | scanner 2 | scanner 3 | scanner 1 | scanner 2 | scanner 3 |
| Pellet I Defect | 37.85 | *27.89 | 41.27 | 13 | *3,022 | 7 | *9.942 | 22.085 | *9.172 |
| Pellet II Defect | *33.68 | 40.57 | 41.63 | *219 | 21 | *1,901 | *17.158 | 37.272 | 23.763 |
| Pellet III Defect | *35.54 | 41.79 | *36.21 | *1,543 | 11 | 5 | *20.914 | *19.646 | 29.325 |

### 4.3.2 Test Results: Defect 2

The testing for the pseudo pellets with the simulated crack defects were carried out next. The crack defects were simulated in the circumferential and longitudinal orientations as well as in multiple occurrences. The results for all three types of scanners can be seen in Table 4.2. It was not possible to produce cracks in the pseudo pellets, so the cracks appear as cuts in the surface of the pellets. The 2D scanner showed less than expected results at detecting crack type defects, especially when measuring a circumferential defect. The 2D scanner had difficulty detecting a circumferential defect, but the lengthwise cracks show up well in the scans; which were found to have an area below 36.8 $mm^2$. Alternatively, the CCD scan is able to detect crack type defects in any orientation, including both large and small sized defects. It can be seen from the results that cracks can be detected from 800 - 1,700 pixels. Also the ability to detect multiple cracks is available using the CCD scan. The Ra scanner was shown to be unreliable at detecting the crack defect unless it passes within the measurement region. The crack type of defect appears as an abnormally low measurement value, less than 21.8 $\mu$-inches, from the surface roughness measurement if it does cross through the scanning region.

Table 4.2: Testing Results for Defect 2: Crack

| Type of Scanner | 2D Scanner ($mm^2$) | | | CCD Scanner (pixels) | | | Ra Scanner($\mu$-inches) | | |
|---|---|---|---|---|---|---|---|---|---|
| Number of Scanner | scanner 1 | scanner 2 | scanner 3 | scanner 1 | scanner 2 | scanner 3 | scanner 1 | scanner 2 | scanner 3 |
| Pellet I Defect | 36.83 | 41.12 | *39.7 | 20 | 9 | *837 | *19.589 | *18.076 | 27.241 |
| Pellet II Defect | 37.04 | *40.98 | 41.06 | *1,677 | 17 | *1,481 | *16.370 | *15.790 | *20.927 |
| Pellet III Defect | *36.33 | 41.72 | 41.82 | *1,588 | 6 | 8 | *17.127 | *16.757 | 21.872 |

### 4.3.3 Test Results: Defect 3

The next types of defects to be tested were the pseudo pellets with simulated end square defects. This type of defect occurs at the ends of the pellets and has been simulated in both aggressive defects and slight ones; only occurring at one end of each pellet. The measured results of the simulated defects are shown in Table 4.3. The defect shows up well in at least one of the 2D scanners and sometimes for multiple ones if the defect appears in more than one of the viewing windows. The measured data is noticeably different from the expected normal trailing or leading edge of the pellet, the results indicating that a value under 40 $mm^2$ is achieved before it is expected. The CCD scanner can identify a large or small defect near the end of the pellet in the presence of an end square defect, depending on the severity of the end square defect. The defect shows up as a large and continuous mass of pixels located at either one end of the pellet or the other. The defects can be captured by more than one scanner depending on the orientation of the pellet to the viewing windows. The end square defects were measured to be as small as 300 pixels and as large as 1,500 pixels. The Ra scanner is more or less unable to detect the end square defect unless it is of sufficient severity and size to be picked up by the scanner before it reaches the end of the pellet. If the scanner is able to pass over a large enough defect, it will show up in the measurement as a lower than expected surface roughness, below 20 $\mu$-inches and above 50 $\mu$-inches. A higher than expected surface roughness was measured during scans of this type of defect, opening the possibility of defects being detected as either higher or lower than expected surface roughness.

Table 4.3: Testing Results for Defect 3: End Squares

| Type of Scanner | 2D Scanner ($mm^2$) | | | CCD Scanner (pixels) | | | Ra Scanner($\mu$-inches) | | |
|---|---|---|---|---|---|---|---|---|---|
| Number of Scanner | scanner 1 | scanner 2 | scanner 3 | scanner 1 | scanner 2 | scanner 3 | scanner 1 | scanner 2 | scanner 3 |
| Pellet I Defect | 38.11 | *40.68 | *39.13 | *324 | 13 | *1,027 | 32.197 | *15.742 | *19.576 |
| Pellet II Defect | 37.92 | 41.78 | *38.25 | 14 | *1,345 | 9 | *17.143 | *19.629 | 23.660 |
| Pellet III Defect | 38.35 | 42.3 | *36.6 | 22 | 7 | *976 | *17.724 | 24.265 | 27.222 |

### 4.3.4 Testing Results: Defect 4

The next testing was done on two types of defects that were identified to be in the same category, which are pits and inclusions. The results of measured defects of the simulated pseudo pellets for both the inclusions and pits can be found in Table 4.4. The 2D scanner showed some success in detecting pits and inclusions of larger size, but smaller sized defects of this type were difficult to detect. The results of the measurement for the smaller sized defects are indiscernibly small from the measurement of the area, acquiring both 37 $mm^2$ and 41 $mm^2$ surface measurements. There is a possibility that the defects are being detected as a very small difference in the measurement, however there is no way to discern this without incorporating historical data. It could be possible to perform an analysis of multiple points or measurement instead of calculating the area in order to detect defects below 1 mm in length or width. Alternatively, the CCD scanner is able to locate single or multiple defects of varying size. The inclusions of very small size do not reveal well during the CCD measurement and show up as negligibly small groupings of pixels in some instances. If there are many small sized negligible defects or defects that border on the rejection threshold, then the results should be compared to the values from the other scanners to identify if pits or inclusions may be present. The larger of the small defects show up well in the CCD scans as groupings of pixels from around 70 - 200 pixels. These larger defects can also be identified with the Ra scanner, but the defect must pass through the scanning area similar to the other types of defects. These values appear as abnormally smooth surfaces, between 16 - 19 $\mu$-inches. It is not reliable to expect the surface roughness scanner to detect any kind of pit or inclusion

defect, as they were rarely detected.

Table 4.4: Testing Results for Defect 4: Inclusions and Pits

| Type of Scanner | 2D Scanner ($mm^2$) | | | CCD Scanner (pixels) | | | Ra Scanner($\mu$-inches) | | |
|---|---|---|---|---|---|---|---|---|---|
| Number of Scanner | scanner 1 | scanner 2 | scanner 3 | scanner 1 | scanner 2 | scanner 3 | scanner 1 | scanner 2 | scanner 3 |
| Pellet I Defect | 37.74 | 41.6 | 42.11 | *77 | 22 | *75 | 23.619 | *18.047 | 24.482 |
| Pellet II Defect | 37.53 | 41.31 | 41.83 | 18 | *158 | 9 | *17.291 | *19.157 | 26.603 |
| Pellet III Defect | 37.27 | *41.68 | 42.47 | 14 | 7 | *132 | *16.715 | *16.584 | 21.464 |

### 4.3.5 Test Results: Defect 5

The second to last defect tests were carried out on pseudo pellets with simulated wheel marks type defects. This defect is simulated by creating flat spots on the surface of the pellet where the surface has unwanted machining marks. The results of the scans that were done for the wheel mark type of defect are presented in Table 4.5. The defective areas on the surface of the pellet changed the otherwise radial cross-section of the pellet. This was expected to create a noticeable difference in the calculated area of the cross-section, however, a lower than expected deviation in the area measurement was realized, 36.02 $mm^2$ and 39.73 $^2$. The CCD scanner was able to clearly identify the wheel mark type of defect; which appears as a large continuous grouping of pixels of about 2,000 pixels, with minimal normal surface areas within the defective area. Similarly to the other larger defects that can occur, the Ra scanner has shown effectiveness at detecting the wheel mark defect as long as it passes through the relatively small scanning area. Depending on the simulated defect, the results showed that either a very rough or a much smoother than expected surface is realized, approximately 14 - 18 $\mu$-inches for smooth surfaces and as high as 68 $\mu$-inches for the very rough surface.

### 4.3.6 Test Results: Defect 6

The last type of defect that was examined, was the simulated non-cleanup defect. This defect was difficult to simulate on the pseudo pellets, since the finish of the pellets is

Table 4.5: Testing Results for Defect 5: Wheel Mark

| Type of Scanner | 2D Scanner ($mm^2$) | | | CCD Scanner (pixels) | | | Ra Scanner($\mu$-inches) | | |
|---|---|---|---|---|---|---|---|---|---|
| Number of Scanner | scanner 1 | scanner 2 | scanner 3 | scanner 1 | scanner 2 | scanner 3 | scanner 1 | scanner 2 | scanner 3 |
| Pellet I Defect | 37.69 | *39.73 | 41.9 | *2,456 | 23 | 12 | *68.908 | 28.065 | 22.105 |
| Pellet II Defect | *36.02 | 42.48 | 41.24 | 19 | 13 | *2,013 | *16.103 | 24.484 | 20.660 |
| Pellet III Defect | 36.67 | 41.45 | 41.22 | *2,071 | 8 | 11 | *18.431 | *14.715 | 20.273 |

smooth and the defect affects the finish of the pellets. The results of the three types of scanners from the three defect pellets can be seen in Table 4.6. Neither the 2D scan nor the CCD scan were able to achieve any discernable values to indicate that a defect was present on any of the three pellets. This is because the altered finish of the pseudo pellet did not really change the surface shape, nor did it show up as large enough defects in the CCD scan. It could be possible to use historical data to find a difference in surface measurements of 2D and CCD scans to indicate the presence of non-cleanup defects. However, the Ra scanner was able to detect the surface of a non-cleanup as a rougher or smother than expected surface. The rough surfaces appeared to be between 33 - 41 $\mu$-inches and above, while the smoother surfaces measured as low as 2 - 20 $\mu$-inches.

Table 4.6: Testing Results for Defect 6: Non-Cleanups

| Type of Scanner | 2D Scanner ($mm^2$) | | | CCD Scanner (pixels) | | | Ra Scanner($\mu$-inches) | | |
|---|---|---|---|---|---|---|---|---|---|
| Number of Scanner | scanner 1 | scanner 2 | scanner 3 | scanner 1 | scanner 2 | scanner 3 | scanner 1 | scanner 2 | scanner 3 |
| Pellet I Defect | 37.5 | 42.18 | 41.68 | 6 | 8 | 11 | *19.955 | *40.849 | *2.516 |
| Pellet II Defect | 37.33 | 41.4 | 41.04 | 12 | 13 | 17 | *17.576 | *15.477 | 32.879 |
| Pellet III Defect | 37.46 | 41.5 | 41.43 | 8 | 7 | 22 | 21.070 | 29.911 | *12.952 |

## 4.4 Summary

The defect scanning tests were necessary to prove the validation of the choice in scanning devices. The types of scanners were reviewed in order to highlight the features present in each scanner that would be useful in detecting surface defects. The testing was carried out on six sets of pseudo pellets; each set of pellets present a variation on the types of defects. These defects were purposely made to be small or

hard to detect, to test the maximum capabilities of the scanners to each ones ability. It has been shown in previous testing documentation that larger sizes or occurrences of defects are more easily noticed than small and difficult to distinguish ones.

The results show that the 2D scanners were able to identify some of the smaller defects, though some results were not as expected; such as the pits and inclusions. In particular the values for the 2D scanners were found to best detect chips and end-squares. Also based on the size difference of the viewing windows, the results of the 2D scans differ from each other as was indicated in the validation found in Chapter 3.

The CCD scanners were able to recognize all of the types of defects to some degree, with the exception of non-cleanups, though some defects such as small inclusions would tend to be classified as negligible defects. A method of comparing the historical results of the CCD scanner to the current scanned results should be devised in order to make appropriate decisions for smaller sized defects.

Finally, the Ra scanner was able to detect surface roughness, unfortunately the simulated surface of the pseudo pellets was less than uniform at this precision. This caused the results to not be at the desired threshold for production, though it appears to be close, which is irrelevant for the simulated defects. Unexpectedly the surface roughness scanner was able to detect most defects, as long as they passed through the viewing area. It must be noted that defects appear as a rougher than expected surface as well as a smoother than expected surface.

The test results have reaffirmed the validation of scanner choices and have revealed some unknown characteristics of the scanners while examining the six indicated types of defects. The use of the three scanning technologies should enable the inspection for all of the identified types of defects.

# Chapter 5

# Conclusions and Recommendations for Future Work

A brief review of the contributions of this thesis and an outline for future works that have been identified, will be presented. This is done in order to conclude this work and give the reader an idea of the final goals of the design; in order to provide a starting point for additional work to be done on this project. The main contributions were the definition of project requirements, the literature research, the validation of design concept and technology that was used, and the test results of scanning a variation of pseudo defective pellets. The design contributions have been discussed in a separate report for the purposes of confidentiality, the reader should refer to [1] for further information. The final contributions will serve as a guide to direct further work for this project and present ideas that have yet to be included in the prototype, in order to produce a viable scanning system for implementation in a production environment. These sections will be divided into a conclusion and future works section.

## 5.1 Conclusions

This work set out to complete the goal of creating and testing an automated scanning system, which has been achieved, as well as constructing a prototype for testing purposes; which has been detailed in another document [3]. The results of the validation and tests of this system were presented. The value in this thesis is that it has identified the problems and design requirements that must be fulfilled for a successful design. This details in particular the specific need for undertaking this project and what problems need to be solved. These particulars were fulfilled by developing a project organization, which included literature research, design of a system to fulfill the identified requirements, and validation and quantification of the scanner results from testing. The available resources were searched for relevant designs, literature, and technology. This namely revealed relevant scanning technologies that are applicable to finding surface defects on cylindrical objects. Also, existing designs were reviewed to provide a starting point for the design process and to provide a baseline on which to gauge improvement and novelty on existing designs. This information made it possible to identify viable devices and scanners that were relevant to fulfilling the design goals of the project.

The contributions of this work have gone further, validating the design concept and scanning technologies that were chosen via a prototype test bed. This part of the research correlates to the design of the system as it chooses the scanners that are to be used in the design and then tests them based on the results of the design.

A set of quantifiable calculations is presented for validation with actual scan results. The calculations correlated to the actual calibrated scan results for each of the chosen technologies from the scanning system design. This shows that the scans for surface shape, surface integrity, and surface roughness are credible and reliable for assessing the surface of the pellets. In addition, the method for calibrating each of the scanners has been presented.

The calibrated system was used to test pseudo defective pellets, which were an attempt to mimic the actually defective pellets as close as possible without testing on actual pellets. This was to ensure that the system is capable of performing the scans before it is subjected to uranium fuel pellets.

The results show that a system of this design will be functional in determining the various qualities of pellets and different severities of defects. Currently, the defect detection is able to record scanner results and compare these results to a threshold giving a decision for each scan that occurs. These results quantify the different sizes of defects found on the pseudo defective pellets, showing that the same could be done for the actual fuel pellets. Based on the research, design, and testing it can be concluded that this is a novel and valid design for the purpose of detecting surface defects on fuel pellets.

## 5.2 Future Work

The continuation of this work will be the further development of the prototype to a working factory model. In order to develop a factory ready model a number of future developments, that lie outside the scope of this project, will need to be undertaken. Currently, there are some critical features that have been identified for development. The first consideration that should be addressed is the implementation of a new camera system, for the scan of surface integrity. Currently the prototype utilizes an adequate CCD and capture card. This system proves that using camera systems to detect defects in the specified manner works well. However, the current system does not incorporate well with the rest of the system components. The current camera system setup has limited communication with the main program and the required values for the defects are difficult to acquire. A camera system that can be programmed directly from the source code would be preferable. The system should

be upgraded to a more modern and developer friendly system and not a standalone solution.

In addition to the above, the processing power of the system can be divided up amongst more PC stations instead of the current single PC setup; in order to improve run time of programs that control the acquisition of measurement values. The computers can be networked instead of using local communications, over sockets and all devices should be accessed by the same level of source code which creates a more harmonized design.

If it is possible a method of validating the test results should be devised. This would have to involve manually quantifying defect measurements and then comparing the results of the actual measurements of the same defects. This would further validate the effectiveness of each type of scanner at detecting each of the categories of different types of defects.

The next area for development will be to test on authentic fuel pellets, in order to calibrate the system and perform the same defect detection tests that were performed in this thesis. The system has been proven with the prototype and now it should be tested to assess whether or not there are any unforeseen problems examining actual reactor bound sintered $UO_2$ pellets. This will be useful in identifying any issues that could present themselves, that are not present when assessing the surfaces of the pseudo pellets.

In this thesis three scanning technologies have been discovered, that will assess the surface characteristics of pellets in a non-contact NDT method. There are still other techniques that were reviewed that are relatively untested for this application, either because they were hard to access or did not satisfy some of the design requirements. It may be possible to validate other technologies that may be suitable for this application. Further work would have to be done in order to show whether or not this is possible.

Finally, testing can be done on the optimization and timings of the system, this will identify the best way to manage the system to keep up with a production scenario.

# References


[1] J. Vanderlaan and S. Nokleby, "Design and Development of an Automated High Speed Inspection System for Uranium Fuel Pellets," Confidential Technical Report, University of Ontario Institute of Technology, Oshawa, ON, October 2011.

[2] J. Vanderlaan and S. Nokleby, "Automated Pellet Inspection: Customer Requirements," Confidential Technical Report, University of Ontario Institute of Technology, Oshawa, ON, December 2008.

[3] Zircatec Precision Inductries Inc., "Quality Verification Instruction: Fuel Stack Inspection," Customer Requirements Document, University of Ontario Institute of Technology & Zircatec Precision Industries, Port Hope, ON, November 2008.

[4] E. Lehmann, G. Frei, S. Hartmann, R. Seiler, and P. Bourquin, "The Inspection of Fresh Nuclear Fuel With The Method of Neutron Imaging," Tech. Rep., Paul Scherrer Institute and Laboratory for Reactor Physics and Systems Behavious, Villigen PSI, Switzerland.

[5] S. Muralidhar, J. P. Panakkal, and A. V. R. Reddy, "A Review On The Development Of Enrichment Scanners For Plutonium And Experimental Uranium Nuclear Fuels," *In BARC Newsletter*, vol. 307, pp. 2–10, August 2009.

[6] I. Badawy, W. A. El-Gammal, and M. Abo-El-Khier, "A non-destructive assay system for the verification of uranium fuel rods," in *Proceedings Of The*

*Thirteenth National Radio science Conference*. IEEE, March 19-21, 1996, pp. 1[H3]–8[H3].

[7] J. P. Panakkal, D. Mukherjee, and H. S. Kamath, "Nondestructive evaluation of uranium-plutonium mixed oxide (mox) fuel elements by gamma autoradiography," in *17th World Conference on Nondestructive Testing*. Bhabha Atomic Research Centre, 25-28 October 2008, pp. 1–9.

[8] P. L. Swart, B. M. Lacquet, and C. Blom, "An acoustic sensor system for determination of macroscopic surface roughness," in *Transactions of Instrumentation and Measurement, Vol. 45, NO. 5*. IEEE, 1996, pp. 879–884.

[9] R. P. Courtney, B. W. Drinkwater, S. A. Neild, and P. D. Wilcox, "Factors affecting the ultrasonic intermodulation crack detection technique using bispectral analysis," in *NDT and E International 41*. Elsevier Limited, 2008, pp. 223–234.

[10] J. P. Panakkal, J. K. Gosh, and P. R. Roy, "Use of Ultrasonic Velocity For Measurement Of Density Of Sintered," *Journal of Physics D: Applied Physics (1995)*, , no. 17, pp. 1791–1795, 1984.

[11] S. K. Nayar, K. Ikeuchi, and T. Kanade, "Surface refelction: Physical and geometrical perspectives," in *Transactions On Pattern Analysis And Machine Intelligence, Vol. 13, NO. 7*. IEEE, July 1991, pp. 611–634.

[12] S. A. Whitehead, A. C. Shearer, D. C. Watts, and N. H. F. Wilson, "Comparison of methods for measuring surface roughness of ceramic," *Journal of Oral Rehabilitation (1995)*, , no. 22, pp. 671–684, 1995.

[13] K. I. Jolic, C. R. Nagarajah, and W. Thompson, "Non-contact, optically based measurement of surface roughness of ceramics," Measurement science and technology 5, Swinburne University of Technology and University of New South Wales, 1994.

[14] S. A. Stefani, C. R. Nagarajah, and R. WIllgoss, "A Surface Inspection Technique For Continuously Extruded Cylindrical Products," Measurement science and technology 10, Swinburne University of Technology and University of New South Wales, 1999.

[15] L. V. Finogenov, A. V. Beloborodov, V. I. Ladygin, Chugui Y. V., N. G. Zagoruiko, Y. S. Gulyaevskii, S. Y. Shul'man, P. I. Lavrenyuk, and Y. V. Pimenov, "An Optoelectronic System For Automatic Inspection Of The External View Of Fuel Pellets," *Russian Journal of Nondestructive Testing*, vol. 43, no. 10, pp. 692–699, 7 June 1997.

[16] J. Lichauer and L. Zana, "Automated Fuel Pellet Inspection System," Society of photographic instrumentation engineers vol. 1823, Westinghouse Electric Corporation Science And Technology Center, 1992.

[17] D. Fischer, S. W. F. Poehlman, and B. Szabados, "Using a bayes classifier to optimize the alarm generation of electric power generator stator overheating," *In IEEE Transactions on Instruments and Measurements*, vol. 52, no. 3, 2003.

[18] M. T. Hayajneh and S. M. Radaideh, "Monitoring hole quality in a drilling process using a fuzzy subtractive clustering-based system identificaion method," *In the Journal of Testing and Evaluation*, vol. 35, no. 3, pp. 1–6, 2006.

[19] S. Keyvan, X. Song, and M. Kelly, "Nuclear Fuel Pellet Inspection Using Artificial Neural Networks," *In the Journal of Nuclear Materials*, vol. 264, pp. 141–154, 1999.

[20] D. J. Hill, "Method for determining nuclear reactor fuel pellet density using gas displacement," US Patent, No. 5,583,897, 10 December 1996.

[21] W. H. Miller Jr., "Automatic inspection system for nuclear fuel pellets or rods," US Patent, No. 4,098,408, 4 July 1978.

[22] S. W. Wilks, "Pellet length and end squareness inspection apparatus," US Patent, No. 4,138,821, 13 February 1979.

[23] H. J. Ahmed, "Nuclear fuel pellet surface defect inspection," US Patent, No. 4,978,495, 18 December 1990.

[24] M. Q. Clark, "Inspecting the surface of an object," US Patent, No. 5,991,017, 23 November 1999.

[25] Y. Nakagawa, "Surface detect test apparatus," US Patent, No. 4,162,126, 24 July 1979.

[26] H. Makihira and Y. Nakagawa, "Method and apparatus for appearance inspection," US Patent, No. 4,410,278, 18 October 1983.

[27] F. C. Schoenig Jr., L. N. Grossman, C. C. Lai, W. Masaitis, and R. O. Canada, "Automated inspection system," US Patent, No. 4,496,056, 29 January 1985.

[28] H. J. Ahmed, J. M. Beatty, and R. W. Kugler, "Pellet inspection system," US Patent, No. 5,147,047, 15 September 1992.

[29] Y. Yaginuma, "Apparatus for inspecting peripheral surface of nuclear fuel pellets," US Patent, No. 4,138,821, 13 February 1979.

[30] J. C. Lichauer, L. J. Zana, N. G. Arila, J. M. Beatty, and H. J. Ahmed, "Non-contact flaw detection for cylindrical nuclear fuel pellets," US Patent, No. 5,309,486, 3 May 1994.

[31] A. K. Ainsworth, R. P. Glenville, and I. A. McLean, "Inspection of cylindrical objects," US Patent, No. 5,541,418, 30 July 1996.

[32] A. K. Ainsworth, R. P. Glenville, and I. A. McLean, "Apparatus for the inspection of cylindrical objects having a borescope device," US Patent, No. 5,703,377, 30 December 1997.

[33] Y. Yaginuma, "Cylindrical body inspection apparatus utilizing displacement information and reflected light information," US Patent, No. 5,625,432, 29 July 1997.

[34] NDT Technologies Inc., "Eddy current encircling probe," On the WWW, 2008, URL http://www.ndttechnic.com/qweb/site/products.htm.

[35] General Electric Sensing and Inspection Technologies, "Ultrasonic transducers," On the WWW, 2010, URL http://www.geinspectiontechnologies.com.

[36] Optical Dimensions LLC, "Lasercheck measurement head: 6212-c," On the WWW, 2008, URL http://www.opticaldimensions.com.

[37] Keyence Corporation, "2d laser profile head: Lj-g030," On the WWW, 2009, URL http://www.keyence.ca/products/vision/laser/ljg/ljg.php.